tribute to human health and longevity. In the present study, SAMP mice were used as an aging model because the internal environment of the body of aged animals and their responses to chemopreventive agents are different from those of young animals. The usage of aged animals to investigate the therapeutic and preventive efficacy of chemopreventive agents may produce more predictable results for actual human cancers.

Acknowledgments The authors thank Dr. Jun Yokota of the National Cancer Center for donating the K1735M2 melanoma cells and Dr. Yukihiko Hara of Mitsui Norin Co., Ltd. for providing the Polyphenon70S. The authors also wish to thank all members of the Department of Medical Biochemistry at the University of Shizuoka for supporting the experiments and their helpful advice. This work was supported in part by the Global COE Program of the Ministry of Education, Culture, Sports, Science and Technology, MEXT, Japan.

REFERENCES

1) Mundy G. R., *Nat. Rev. Cancer*, **2**, 584—593 (2002).
2) Anisimov V. N., *Crit. Rev. Oncol. Hematol.*, **45**, 277—304 (2003).
3) Krtolica A., Campisi J., *Int. J. Biochem. Cell Biol.*, **34**, 1401—1414 (2002).
4) Kikkawa H., Tsukada H., Oku N., *Cancer*, **89**, 1626—1633 (2000).
5) Kikkawa H., Imafuku H., Tsukada H., Oku N., *FEBS Lett.*, **467**, 211—216 (2000).
6) Takeda T., Hosokawa M., Higuchi K., *Exp. Gerontol.*, **32**, 105—109 (1997).
7) Higuchi K., *Exp. Gerontol.*, **32**, 129—138 (1997).
8) Miyamoto M., *Exp. Gerontol.*, **32**, 139—148 (1997).
9) Shimizu K., Kinouchi Shimizu N., Asai T., Tsukada H., Oku N., *Biol. Pharm. Bull.*, **31**, 847—851 (2008).
10) Surh Y. J., *Nat. Rev. Cancer*, **3**, 768—780 (2003).
11) Khan N., Afaq F., Saleem M., Ahmad N., Mukhtar H., *Cancer Res.*, **66**, 2500—2505 (2006).
12) Oku N., Matsukawa M., Yamakawa S., Asai T., Yahara S., Hashimoto F., Akizawa T., *Biol. Pharm. Bull.*, **26**, 1235—1238 (2003).
13) Yamakawa S., Asai T., Uchida T., Matsukawa M., Akizawa T., Oku N., *Cancer Lett.*, **210**, 47—55 (2004).
14) Tachibana H., Koga K., Fujimura Y., Yamada K., *Nat. Struct. Mol. Biol.*, **11**, 380—381 (2004).
15) Umeda D., Yano S., Yamada K., Tachibana H., *J. Biol. Chem.*, **283**, 3050—3058 (2007).
16) Koike C., Watanabe M., Oku N., Tsukada H., Irimura T., Okada S., *Cancer Res.*, **57**, 3612—3619 (1997).
17) Benz C. C., Yau C., *Nat. Rev. Cancer*, **8**, 875—879 (2008).
18) Burns E. A., Leventhal E. A., *Cancer Control*, **7**, 513—522 (2000).
19) Campisi J., *Nat. Rev. Cancer*, **3**, 339—349 (2003).
20) Crespy V., Williamson G., *J. Nutr.*, **134**, 3431S—3440S (2004).
21) Mori A., Utsumi K., Liu J., Hosokawa M., *Ann. N.Y. Acad. Sci.*, **854**, 239—250 (1998).
22) Tobi S. E., Gilbert M., Paul N., McMillan T. J., *Int. J. Cancer*, **102**, 439—444 (2002).
23) Nakamura K., Matsunaga K., *Cancer Biother. Radiopharm.*, **13**, 275—290 (1998).
24) Ferrández M. D., Correa R., Del Rio M., De la Fuente M., *Exp. Gerontol.*, **34**, 675—685 (1999).
25) Frei B., Higdon J. V., *J. Nutr.*, **133**, 3275S—3284S (2003).
26) Unno K., Takabayashi F., Yoshida H., Choba D., Fukutomi R., Kikunaga N., Kishido T., Oku N., Hoshino M., *Biogerontology*, **8**, 89—95 (2007).
27) Unno K., Takabayashi F., Kishido T., Oku N., *Exp. Gerontol.*, **39**, 1027—1034 (2004).
28) Shimizu M., Fukutomi Y., Ninomiya M., Nagura K., Kato T., Araki H., Suganuma M., Fujiki H., Moriwaki H., *Cancer Epidemiol. Biomarkers Prev.*, **17**, 3020—3025 (2008).

Analytical Biochemistry 396 (2010) 257–261

Contents lists available at ScienceDirect

Analytical Biochemistry

journal homepage: www.elsevier.com/locate/yabio

Bionanocapsule-based enzyme–antibody conjugates for enzyme-linked immunosorbent assay

Masumi Iijima [a,b], Takashi Matsuzaki [a], Hiroyasu Kadoya [a], Satoko Hatahira [c], Shingo Hiramatsu [c], Giman Jung [c], Katsuyuki Tanizawa [a,*], Shun'ichi Kuroda [a,b,*]

[a] Institute of Scientific and Industrial Research, Osaka University, Ibaraki, Osaka 567-0047, Japan
[b] Graduate School of Bioagricultural Sciences, Nagoya University, Chikusa, Nagoya 464-8601, Japan
[c] New Frontiers Research Laboratories, Toray Industries, Kamakura, Kanagawa 248-8555, Japan

ARTICLE INFO

Article history:
Received 7 July 2009
Available online 9 October 2009

Keywords:
ELISA
IgG
Protein A
Nanoparticles
Oriented immobilization

ABSTRACT

Macromolecules that can assemble a large number of enzyme and antibody molecules have been used frequently for improvement of sensitivities in enzyme-linked immunosorbent assays (ELISAs). We generated bionanocapsules (BNCs) of approximately 30 nm displaying immunoglobulin G (IgG) Fc-binding ZZ domains derived from *Staphylococcus aureus* protein A (designated as ZZ-BNC). In the conventional ELISA using primary antibody and horseradish peroxidase-labeled secondary antibody for detecting antigen on the solid phase, ZZ-BNCs in the aqueous phase gave an approximately 10-fold higher signal. In Western blot analysis, the mixture of ZZ-BNCs with secondary antibody gave an approximately 50-fold higher signal than that without ZZ-BNCs. These results suggest that a large number of secondary antibody molecules are immobilized on the surface of ZZ-BNCs and attached to antigen, leading to the significant enhancement of sensitivity. In combination with the avidin–biotin complex system, biotinylated ZZ-BNCs showed more significant signal enhancement in ELISA and Western blot analysis. Thus, ZZ-BNC is expected to increase the performance of various conventional immunoassays.

Enzyme immunoassay (EIA),[1] radioimmunoassay (RIA), and fluoroimmunoassay (FIA) have been widely used for high-throughput screening of immunocomplexes. To increase the sensitivity of these immunoassays, two types of macromolecules have been used in the reaction with antibody. One type of macromolecule allows clustering of antibodies and labeling molecules (e.g., enzyme, radioactive material, fluorescence). For example, polymeric horseradish peroxidase (HRP)–streptavidin conjugate [1], 3DNA dendrimer [2], and immunoglobulin G (IgG)–poly-D-glutamic acid–$(HRP)_n$ conjugate [3] have been used previously. However, these macromolecules require chemical modification of antibodies and do not allow the oriented immobilization of antibodies [4] that improves the avidity and antigen recognition of antibodies [5]. In general, chemical modification is considered to reduce the stability or antigen-binding activity of antibodies. Another type of macromolecule is expected to permit the oriented immobilization of antibodies. For example, nanoparticles have been used for displaying antibodies on their surface (e.g., streptavidin-conjugated nanobeads [6], biotin-coated liposomes [7]). Because biotinylation occurred randomly at free amino groups on the surface of antibodies, these nanoparticles partially accomplished oriented immobilization of antibodies using a avidin–biotin complex (ABC). These results encouraged us to develop macromolecules that can assemble antibodies and labeling molecules without chemical modification in the manner of oriented immobilization.

On the other hand, we previously developed a yeast-derived hollow nanoparticle applicable for pinpoint delivery of drugs and genes [8]. The nanoparticle, bionanocapsule (BNC), has a diameter of approximately 30 nm and is composed of hepatitis B virus (HBV) surface antigen (HBsAg) L proteins embedded in a liposome [9]. The L protein is a three-membrane-spanning protein possessing a pre-S region at the N terminal of the S region (see Fig. 1A) [10]. BNCs can incorporate various therapeutic materials (e.g., drugs, genes) by electroporation [8] and liposome fusion [11] and can deliver them specifically to the human liver [8] based on the liver-specific recognition ability of the pre-S region [12]. Recently, to alter the tissue specificity of BNC, our collaborators made a

* Corresponding authors. Fax: +81 6 6879 8460 (K. Tanizawa), +81 52 789 5227 (S. Kuroda).
E-mail addresses: tanizawa@sanken.osaka-u.ac.jp (K. Tanizawa), skuroda@agr.nagoya-u.ac.jp (S. Kuroda).

[1] *Abbreviations used:* EIA, enzyme immunoassay; RIA, radioimmunoassay; FIA, fluoroimmunoassay; HRP, horseradish peroxidase; IgG, immunoglobulin G; ABC, avidin–biotin complex; BNC, bionanocapsule; HBV, hepatitis B virus; HBsAg, HBV surface antigen; ZZ-BNC, IgG Fc-interacting region (Z domain) derived from *Staphylococcus aureus* protein A; ELISA, enzyme-linked immunosorbent assay; TEM, transmission electron microscopy; OVA, ovalbumin; PBS, phosphate-buffered saline; TMB, 3,3′,5,5′-tetramethylbenzidine; IgE, immunoglobulin E; PVDF, polyvinylidene fluoride; EGFR, epidermal growth factor receptor; EGFP, enhanced green fluorescent protein; LOD, limit of detection; SD, standard deviations; LOQ, limit of quantitation.

0003-2697/$ - see front matter © 2009 Elsevier Inc. All rights reserved.
doi:10.1016/j.ab.2009.10.010

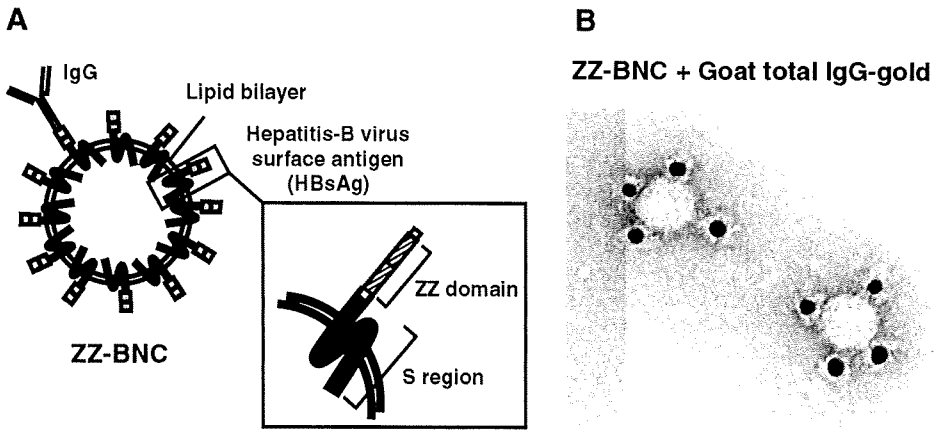

Fig. 1. (A) Schematic structure of a ZZ-BNC. (B) Transmission electron microscopy (TEM) images of ZZ-BNC conjugated with 10-nm gold particle-labeled goat total IgG. Bar = 40 nm.

derivative of BNC by replacing the pre-S region with a tandem sequence of the IgG Fc-interacting region (Z domain) derived from *Staphylococcus aureus* protein A [13] and designated it ZZ-BNC [14] (Fig. 1A). ZZ-BNC allowed us to display antibodies on its surface and to deliver various therapeutic materials to tissues of interest in an antibody-dependent manner [14].

These properties led us to imagine that ZZ-BNC spontaneously adsorbs antibodies in the manner of oriented immobilization. In this study, we examined whether ZZ-BNCs could contribute to signal enhancement of enzyme-linked immunosorbent assay (ELISA) through formation of IgG–ZZ-BNC complexes.

Materials and methods

ZZ-BNCs

ZZ-BNCs were overexpressed in *Saccharomyces cerevisiae* AH22R$^-$ carrying the ZZ-BNC expression plasmid pGLD-ZZ50 [14]. According to the preparation method for BNCs [8], ZZ-BNCs were extracted by the disruption with glass beads and purified using an AKTA chromatography system (GE Healthcare, Amersham, UK) by affinity chromatography on porcine IgG and gel filtration.

Transmission electron microscopy

ZZ-BNCs (1 μg as protein) were mixed with 10-nm gold particle-labeled goat total IgG (50 μl, Sigma–Aldrich, St. Louis, MO, USA), adsorbed onto a carbon-coated copper grid (JEOL, Tokyo, Japan), negatively stained using 2% (w/v) phosphotungstic acid (pH 7.0), and subjected to transmission electron microscopy (TEM) using a model JEM1011 (Jeol).

ELISA for ovalbumin on solid phase

Ovalbumin (OVA, 100 μl, 0–6.25 ng/ml, Sigma–Aldrich) was adsorbed to each well of a Nunc–Immuno Plate II (96 wells, Nalge Nunc International, Rochester, NY, USA). The plate was kept at 4 °C overnight and washed three times with PBST (200 μl of phosphate-buffered saline [PBS], 137 mM NaCl, 2.7 mM KCl, 10 mM Na_2PO_4, and 2 mM KH_2PO_4 [pH 7.4] containing 0.05% [v/v] Tween 20). Antibodies were diluted with PBST containing 5% (w/v) skimmed milk (Nacalai Tesque, Kyoto, Japan). A primary antibody, a mouse anti-OVA IgG_1 antibody (100 μl, 0.4 μg/ml, Abcam, Cambridge, UK), was added to each well, incubated at room temperature for 1.5 h, and washed three times with PBST. A secondary antibody, HRP-conjugated rabbit anti-mouse IgG (100 μl, 2 μg/ml, Sigma–Aldrich), was added to each well, incubated at room temperature for 1.5 h, and washed three times with PBST. When biotinylated rabbit anti-mouse IgG (100 μl, 2 μg/ml, Sigma–Aldrich) was used as the secondary antibody, the ABC system (ABC peroxidase staining kit, Pierce, Rockford, IL, USA) was used for the labeling with HRP. The colorimetric reaction was carried out at room temperature for 15 min in 100 μl per well of a 3,3′,5,5′-tetramethylbenzidine (TMB) substrate kit (Pierce). The reaction was stopped with 100 μl of 2 N H_2SO_4. Absorbance at 450 nm was measured on a Varioskan microplate reader (Thermo Fisher Scientific, Waltham, MA, USA) using absorbance at 690 nm as the reference. When the calibration curve was generated using 0–6.25 ng/ml OVA ($n = 8$), the wells containing 0 ng/ml OVA were defined as blank wells for subtracting background.

ELISA for anti-OVA immunoglobulin E antibodies in aqueous phase

OVA (100 μl, 15 μg/ml) was adsorbed onto each well of a Nunc–Immuno Plate II. The plate was kept at 4 °C overnight and washed three times with 200 μl of PBST. Mouse anti-OVA immunoglobulin E (IgE) antibody (0–6.25 ng/ml, 100 μl, AbD Serotec, Oxford, UK) diluted with PBST containing 5% skimmed milk was added to each well, incubated at room temperature for 1.5 h, and washed three times with PBST. An HRP-conjugated rabbit anti-mouse IgE Fc antibody (100 μl, 5 μg/ml, Nordic Immunological Laboratories, Tilburg, Netherlands) was added to each well, incubated at room temperature for 1.5 h, and washed three times with PBST. When biotin-labeled rabbit anti-mouse IgE Fc antibody (100 μl, 5 μg/ml, Nordic Immunological Laboratories) was used as the secondary antibody, the ABC peroxidase staining kit was used for the labeling with HRP. The colorimetric reaction was carried out at room temperature for 15 min in 100 μl per well of a TMB substrate kit. The reaction was stopped with 100 μl of 2 N H_2SO_4. Absorbance at 450 nm was measured on a Varioskan microplate reader using absorbance at 690 nm as the reference. When the calibration curve was generated using 0–6.25 ng/ml anti-OVA IgE ($n = 8$), the wells containing 0 ng/ml anti-OVA IgE were defined as blank wells for subtracting background.

Western blot analysis

Here 1 μl of OVA (0.001–10 mg/ml) was blotted onto a polyvinylidene fluoride (PVDF) membrane (Millipore, Billerica, MA,

USA) and dried at room temperature for 30 min. The membrane was blocked with 5% skimmed milk in TBST (20 mM Tris–HCl, 140 mM NaCl, and 0.05% Tween 20 [pH 7.4]) at room temperature for 30 min and then incubated at room temperature for 1 h with the mouse anti-OVA IgG_1 antibody (1 μg/ml) diluted with TBST. The membrane was washed three times with TBST and incubated with the HRP-conjugated rabbit anti-mouse IgG (1 μg/ml) at room temperature for 1 h. When biotinylated rabbit anti-mouse IgG (1 μg/ml) was used as the secondary antibody, the ABC system was used for the labeling with HRP. After washing three times with TBST, the membrane was treated with ECL Western blotting detection reagents (GE Healthcare) and then the immunoreactive spots were visualized under a luminescence image analyzer (LAS-4000mini, Fujifilm, Tokyo, Japan).

Results and discussion

Display of antibodies on ZZ-BNC surface

BNC is a yeast-derived hollow nanocapsule consisting of approximately 110 HBsAg L proteins embedded in a liposome [8]. Recently, we replaced the N-terminal region of L protein (pre-S region) with a tandem sequence of protein A-derived IgG Fc-binding domain (Z domain) and designated it ZZ-BNC [14] (Fig. 1A). When mixed with anti-EGFR (epidermal growth factor receptor) antibody, the ZZ-BNCs labeled with enhanced green fluorescent protein (EGFP) accumulated on the surface of human cervical carcinoma HeLa cells that express EGFR abundantly [14]. Therefore, we mixed ZZ-BNC with 10-nm gold particle-labeled goat total IgG and observed it under TEM. As shown in Fig. 1B, approximately 30-nm ZZ-BNCs were surrounded by several molecules of 10-nm gold particle-labeled goat total IgG. This result strongly suggested that ZZ domains surrounding the ZZ-BNC surface tether the IgG Fc domains to display all IgG Fv regions outward for effective antigen binding. Thus, ZZ-BNC was expected to cluster antibodies on its surface in the manner of oriented immobilization, which might improve the avidity and antigen recognition of antibodies [5].

ELISA for antigens on solid phase

The enhancement of the sensitivity was examined in the detection of antigen (OVA) by ELISA with or without ZZ-BNCs (see Fig. 2A, panels 1 and 2). As described in Materials and methods, OVA (0–6.25 ng/ml) was adsorbed onto each well of the immunoplate, contacted with primary antibody, and then contacted with secondary antibody (see Fig. 2A, panel 1). When the purified ZZ-BNCs (2 μg/ml as protein) were preincubated with the secondary antibody (2 μg/ml) at room temperature for 30 min and then added to each well (see Fig. 2A, panel 2), the signal at 3.125 ng/ml OVA was approximately 10-fold higher than that without ZZ-BNCs (Fig. 2B, lines 1 and 2). The ABC system has been widely used for the enhancement of ELISA signals because it forms a tetrameric avidin-based complex of biotinylated antibodies and biotinylated HRP (see Fig. 2A, panel 3). The signal at 3.125 ng/ml OVA with the ABC system was approximately 4-fold higher than that with the conventional ELISA (Fig. 2B, lines 1 and 3). When ZZ-BNC (2 μg/ml as protein) was preincubated with the biotinylated secondary antibody (2 μg/ml) at room temperature for 30 min and then added to each well (100 μl) (see Fig. 2A, panel 4), the signal at 3.125 ng/ml OVA was approximately 13-fold higher than that without ZZ-BNCs or the ABC system (Fig. 2B, lines 1 and 4). Next, biotinylated ZZ-BNCs (2 μg/ml as protein) were prepared with EZ-Link Sulfo-NHS-Biotin (Pierce) according to the manufacturer's protocol and added to the secondary antibody instead of ZZ-BNCs (see Fig. 2A, panel 5). The signal at 3.125 ng/ml OVA was approximately 19-fold higher than that without ZZ-BNCs or the ABC sys-

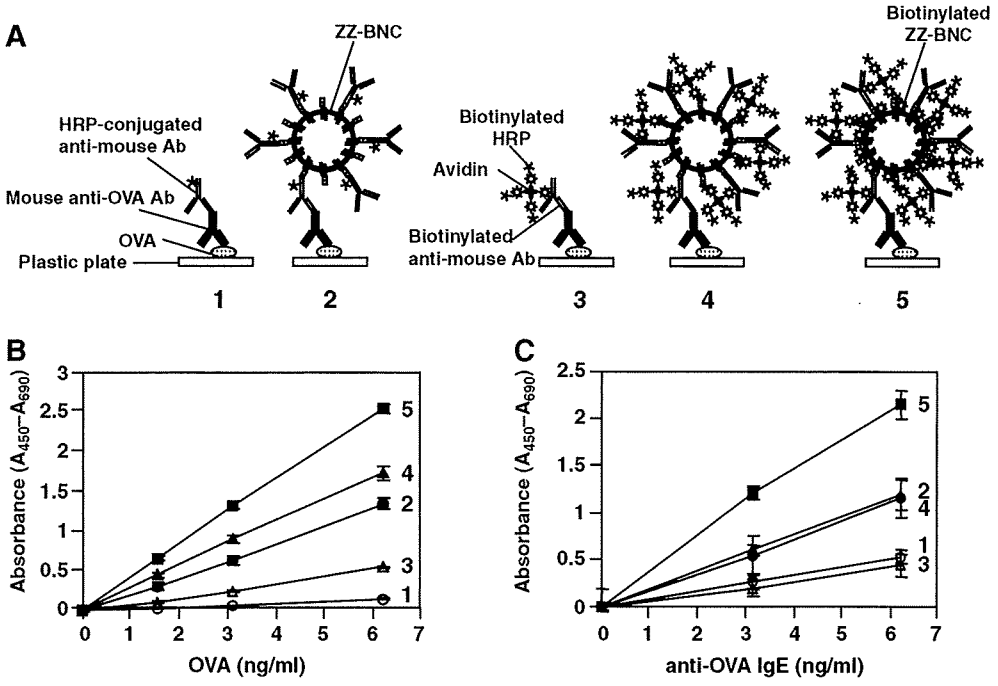

Fig. 2. (A) Schematic representations of various ELISA systems for OVA detection. Panel 1: conventional ELISA using an anti-OVA antibody and an HRP-conjugated anti-mouse IgG antibody; panel 2: conventional ELISA in the presence of ZZ-BNC; panel 3: conventional ELISA with the ABC system; panel 4: conventional ELISA with the ABC system in the presence of ZZ-BNCs; panel 5: conventional ELISA with the ABC system in the presence of biotinylated ZZ-BNC. Ab, antibody. (B) Detection of OVA (solid phase) by various ELISA systems. Results are means ± SD ($n = 8$). Numbers correspond to the methods shown in panel (A). (C) Detection of anti-OVA IgE (aqueous phase) by various ELISA systems. Results are means ± SD ($n = 8$). Numbers correspond to the methods shown in panel (A).

tem (Fig. 2B, lines 1 and 5). The sensitivity for ELISA is defined by the limit of detection (LOD, mean ± 3SD [standard deviations]) and the limit of quantitation (LOQ, mean ± 10SD) [15] at the lowest end of the quantifiable concentration range of OVA ($n = 20$). As shown in Table 1, the LOD and LOQ of ELISA (see Fig. 2A, panel 1, 750 and 1500 pg/ml, respectively) were decreased by 47% using ZZ-BNCs (see Fig. 2A, panel 2, 350 and 700 pg/ml, respectively), indicating that the two sensitivities (LOD and LOQ) were increased 2.1-fold. The ABC system enhanced the two sensitivities 2.5- and 20-fold in the presence of ZZ-BNCs (see Fig. 2A, panel 4) and biotinylated ZZ-BNCs (see Fig. 2A, panel 5), respectively.

ELISA for antibodies in aqueous phase

We investigated the enhancement of the sensitivity of detection of the primary antibody by ELISA using ZZ-BNCs and biotinylated ZZ-BNCs. OVA adsorbed onto each well was contacted with primary antibody (0–6.25 ng/ml) and then contacted with secondary antibody (see Materials and methods and Fig. 2A, panel 1). When ZZ-BNC (1.25 μg/ml as protein) was preincubated with the secondary antibody (5 μg/ml) at room temperature for 30 min and then added to each well (see Fig. 2A, panel 2), the signal at 3.125 ng/ml mouse anti-OVA IgE antibody was 2.3-fold higher than that without ZZ-BNCs (Fig. 2C, lines 1 and 2). Next, with the concurrent use of biotinylated secondary antibody (5 μg/ml), biotinylated ZZ-BNCs (2.5 μg/ml as protein), and the ABC system, the signal at 3.125 ng/ml mouse anti-OVA IgE antibody was 4.4-fold higher than that of conventional ELISA (Fig. 2C, lines 1 and 5). Furthermore, the sensitivity for ELISA is defined by the LOD and LOQ [15] at the lowest end of the quantifiable concentration range of anti-OVA IgE ($n = 20$). The LOD was decreased by 50% and 8% using ZZ-BNCs and biotinylated ZZ-BNCs, respectively (Table 1).

Western blot analysis

Signal enhancement of ELISA for antigens on solid phase by ZZ-BNCs led us to examine whether they are applicable for Western blot analysis. The dot blot containing OVA (from 1 ng/spot to 10 μg/spot) was incubated with the primary antibody at room temperature for 1 h, incubated with the secondary antibody at room temperature for 1 h, and then subjected to chemiluminescence detection (see Materials and methods). When ZZ-BNCs (1 μg/ml as protein) were preincubated with the secondary antibody (1 μg/ml) at room temperature for 30 min, the spot containing 10 ng of OVA could be detected, which was approximately 50-fold higher than that without ZZ-BNCs (Fig. 3, lanes 1 and 2). Next, the use of the ABC system and biotinylated secondary antibody facilitated us to detect the spot containing 50 ng of OVA (Fig. 3, lane 3). The adaptation of ZZ-BNCs (1 μg/ml as protein) and biotinylated ZZ-BNCs (1 μg/ml as protein) to this system achieved approximately 5- and 10-fold higher sensitivity (Fig. 3, lanes 4 and 5, respectively), comparable to 50- and 100-fold enhancements from the conventional method (lane 1). It was confirmed that the combined use of the ABC system and biotinylated ZZ-BNCs significantly enhanced the sensitivity of not only ELISA but also Western blot analysis. Furthermore, ZZ-BNCs might be applicable for the signal enhancement of immunohistochemical analysis.

Table 1
Sensitivities of various ELISA systems for OVA.

Method	LOD (pg/ml) (mean ± 3SD)	CV (%)	LOQ (pg/ml) (mean ± 10SD)	CV (%)
For detection of antigen (OVA)				
Conventional ELISA	750	4.5	1500	3.4
+ ZZ-BNC	350	6.4	700	6.9
+ ABC	500	3.0	1000	3.1
+ ABC + ZZ-BNC	300	5.3	600	11.8
+ ABC + bio-ZZ-BNC	40	3.5	80	4.3
For detection of primary antibody (anti-OVA IgE)				
Conventional ELISA	500	5.0	ND	ND
+ ZZ-BNC	250	5.4	500	4.6
+ ABC + bio-ZZ-BNC	40	4.2	130	3.6

Note. bio-, biotinylated; ND, not detected.

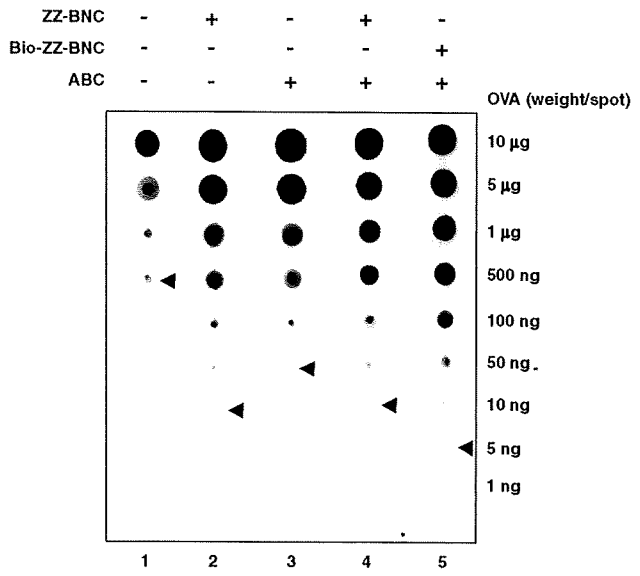

Fig. 3. Western blot analyses of spotted OVA by various detection methods. Lane numbers correspond to the methods shown in Fig. 2A. The minimum OVA amounts detectable by each method are indicated with arrowheads.

Conclusions

It has been demonstrated that ZZ-BNCs could assemble antibodies on their surface even without chemical modification. ZZ-BNCs could then enhance the signals in the detection of antigens and antibodies when added to the aqueous phase of conventional ELISA and Western blot analysis. A combination of the ABC system and biotinylated ZZ-BNCs significantly improved the sensitivity of conventional ELISA and Western blot analysis. In Fig. 1B, ZZ-BNCs are shown to tether the Fc regions of IgG on the ZZ domain so that all of the Fv regions are displayed outward for effective formation of immunocomplexes. Thus, oriented immobilization of antibodies has presumably been achieved on the surface of ZZ-BNCs. As mentioned above, BNCs (including ZZ-BNCs) can incorporate various materials by electroporation and liposome fusion. This indicated that ZZ-BNCs may be applicable for RIA and FIA. BNCs could be adsorbed onto a mica surface without the disruption of its particle structure [16]. Therefore, ZZ-BNCs would also be applicable for the oriented immobilization of antibodies in the solid phase of various immunoassay systems.

Acknowledgments

We thank Profs. A. Kondo (Kobe University), M. Seno (Okayama University), and M. Ueda (Keio University) for helpful advice. This work was supported by the Research and Development Program for New Bio-industry Initiatives from the Bio-oriented Technology Research Advancement Institution (BRAIN) of Japan; the Research on Advanced Medical Technology from the Ministry of Health,

Labor, and Welfare of Japan; and the Regional Research and Development Resources Utilization Program of the Japan Science and Technology Agency (JST).

References

[1] R.G. Vasilov, E.N. Tsitsikov, An ultrasensitive immunoassay for human IgE measurement in cell-culture supernatant, Immunol. Lett. 26 (1990) 283–284.
[2] J.R. Mora, T.L. Zielinski, B.P. Nelson, R.C. Getts, Protein detection enhanced by 3DNA dendrimer signal amplification, BioTechniques 44 (2008) 815–818.
[3] B. Simons, H. Kaplan, M.A. Hefford, Novel cross-linked enzyme–antibody conjugates for Western blot and ELISA, J. Immunol. Methods 315 (2006) 88–98.
[4] S.V. Rao, K.W. Anderson, L.G. Bachas, Oriented immobilization of proteins, Mikrochim. Acta 128 (1998) 127–143.
[5] N.S. Lipman, L.R. Jackson, L.J. Trudel, F. Weis-Garcia, Monoclonal versus polyclonal antibodies: distinguishing characteristics, applications, and information resources, ILAR J. 46 (2005) 258–268.
[6] Y. Teramura, Y. Arima, H. Iwata, Surface plasmon resonance-based highly sensitive immunosensing for brain natriuretic peptide using nanobeads for signal amplification, Anal. Biochem. 357 (2006) 208–215.
[7] T. Wink, S.J. van Zuilen, A. Bult, W.P. van Bennekom, Liposome-mediated enhancement of the sensitivity in immunoassays of proteins and peptides in surface plasmon resonance spectrometry, Anal. Chem. 70 (1998) 827–832.
[8] T. Yamada, Y. Iwasaki, H. Tada, H. Iwabuki, M.K. Chuah, T. VandenDriessche, H. Fukuda, A. Kondo, M. Ueda, M. Seno, K. Tanizawa, S. Kuroda, Nanoparticles for the delivery of genes and drugs to human hepatocytes, Nat. Biotechnol. 21 (2003) 885–890.
[9] S. Kuroda, S. Otaka, T. Miyazaki, M. Nakao, Y. Fujisawa, Hepatitis B virus envelope L protein particles, J. Biol. Chem. 267 (1992) 1953–1961.
[10] T. Nagaoka, T. Fukuda, S. Yoshida, H. Nishimura, D. Yu, S. Kuroda, K. Tanizawa, A. Kondo, M. Ueda, H. Yamada, H. Tada, M. Seno, Characterization of bionanocapsule as a transfer vector targeting human hepatocyte carcinoma by disulfide linkage modification, J. Control. Release 118 (2007) 348–356.
[11] J. Jung, T. Matsuzaki, K. Tatematsu, T. Okajima, K. Tanizawa, S. Kuroda, Bionanocapsule conjugated with liposomes for in vivo pinpoint delivery of various materials, J. Control. Release 126 (2008) 255–264.
[12] A.R. Neurath, S.B. Kent, N. Strick, K. Parker, Identification and chemical synthesis of a host cell receptor binding site on hepatitis B virus, Cell 46 (1986) 429–436.
[13] B. Nilsson, T. Moks, B. Jansson, L. Abrahmsén, A. Elmblad, E. Holmgren, C. Henrichson, T.A. Jones, M. Uhlén, A synthetic IgG-binding domain based on staphylococcal protein A, Protein Eng. 1 (1987) 107–113.
[14] N. Kurata, T. Shishido, M. Muraoka, T. Tanaka, C. Ogino, H. Fukuda, A. Kondo, Specific protein delivery to target cells by antibody-displaying bionanocapsules, J. Biochem. 144 (2008) 701–707.
[15] D. MacDougall, W.B. Crummett, Guidelines for data acquisition and data quality evaluation in environmental chemistry, Anal. Chem. 52 (1980) 2242–2249.
[16] T. Kanno, T. Yamada, H. Iwabuki, H. Tanaka, S. Kuroda, K. Tanizawa, T. Kawai, Size distribution measurement of vesicles by atomic force microscopy, Anal. Biochem. 309 (2002) 196–199.

Available online at www.sciencedirect.com
ScienceDirect
ELSEVIER
Nanomedicine: Nanotechnology, Biology, and Medicine xx (2010) xxx–xxx
nanomedicine
www.nanomedjournal.com

Research Article: Medicine

Hepatoma-targeted gene delivery using a tumor cell–specific gene regulation system combined with a human liver cell–specific bionanocapsule

Jeong-Hun Kang, PhD[a,1], Jun Oishi, PhD[a,b,1], Jong-Hwan Kim, PhD[c], Moeko Ijuin, MD[a,b], Riki Toita, MD[a,b], Byungdug Jun, PhD[c], Daisuke Asai, PhD[d], Takeshi Mori, PhD[a,b], Takuro Niidome, PhD[a,b,e], Katsuyuki Tanizawa, PhD[f], Shun'ichi Kuroda, PhD[f], Yoshiki Katayama, PhD[a,b,e,*]

[a]*Department of Applied Chemistry, Faculty of Engineering, Kyushu University, Fukuoka, Japan*
[b]*Graduate School of Systems Life Sciences, Kyushu University, Fukuoka, Japan*
[c]*Faculty of Education, Nagasaki University, Nagasaki, Japan*
[d]*Department of Microbiology, St. Marianna University School of Medicine, Kawasaki, Japan*
[e]*Center for Future Chemistry, Kyushu University, Fukuoka, Japan*
[f]*Institute of Scientific and Industrial Research, Osaka University, Osaka, Japan*

Received 4 July 2009; accepted 15 January 2010

Abstract

Hepatoma (hepatocellular carcinoma) is the most common type of malignant tumor originating in the liver and has a relatively low 5-year survival rate. The development of hepatoma-targeted therapy is needed to increase treatment efficiency and to reduce the incidence of undesirable side effects. In this study we developed a novel hepatoma-targeted gene delivery system. The gene delivery system was prepared by combining a human liver cell–specific bionanocapsule (BNC) and a tumor cell–specific gene regulation polymer, which responds to hyperactivated protein kinase Cα in hepatoma cells. The complex of the polymer-DNA with BNCs was delivered into cells and tissues. The developed system showed increased transfection efficiency and resulted in cell-specific gene expression in hepatoma cells and tissues (HuH-7), but no gene expression in normal human hepatocytes or human epidermoid tumor cells (A431). The combination of a tumor cell-specific gene regulation system responding to protein kinase Cα and BNCs showed excellent potential for the selective treatment of hepatomas. The system could be a useful method with applications in hepatoma-specific gene therapy and molecular imaging.

Key words: Protein kinase; Intracellular signal; Hepatocellular carcinoma; Gene delivery

Hepatoma (hepatocellular carcinoma) is the most common type of malignant tumor originating in the liver and has a relatively low 5-year survival rate (<10%).[1,2] It is highly resistant to conventional chemotherapy and radiation therapy. Moreover, because many conventional antitumor drugs are nonselective for hepatoma cells, they can cause undesirable side effects.[3,4]

There has been a recent increase in interest in gene therapy as a new approach to hepatoma treatment. Viral and nonviral vectors are used to deliver therapeutic genes, mainly tumor suppressor (e.g., p53) and suicide genes (e.g., herpes simplex virus thymidine kinase), into hepatoma cells. However, problems arise, because the delivered gene is expressed both in targeted hepatoma cells and in nontargeted normal cells. Many targeting strategies using hepatoma-specific molecular markers, mainly membrane receptors, have been investigated with the aim of overcoming this problem.[5-8]

Our group has investigated the possible application of intracellular signal transduction pathways for disease-targeted

This work was supported in part by a Grant-in-Aid for Scientific Research from the Ministry of Education, Science, Sports and Culture of Japan.

*Corresponding author: Department of Applied Chemistry, Faculty of Engineering, Kyushu University, 744 Motooka, Nishi-Ku, Fukuoka 819-0395, Japan.
E-mail address: ykatatcm@mbox.nc.kyushu-u.ac.jp (Y. Katayama).
[1] These authors contributed equally to this work.

1549-9634/$ – see front matter © 2010 Elsevier Inc. All rights reserved.
doi:10.1016/j.nano.2010.01.007

Please cite this article as: J.-H., Kang, et al, Hepatoma-targeted gene delivery using a tumor cell–specific gene regulation system combined with a human liver cell–specific bionanocapsule. *Nanomedicine: NBM* 2010;xx:1-7, doi:10.1016/j.nano.2010.01.007

gene therapy.[9-11] Living cells make use of numerous intracellular signal transduction pathways that respond to extracellular signals and regulate or modulate gene expression. Phosphorylation by protein kinases has an important role in cellular growth and functions through activation of their target proteins in these intracellular signal transduction pathways. Abnormal activation of certain protein kinases has been reported in many diseases.[12,13] If such hyperactivated protein kinases can be used to activate transgene expression, disease cell-specific gene regulation becomes possible.

Among the protein kinases, protein kinase C (PKC) is a phospholipid-dependent serine/threonine kinase that seems to be involved in the signal transduction response to a variety of hormones and growth factors. PKC isozymes are classified into three subfamilies based on structural and activational characteristics: conventional or classic PKCs (cPKCs; α, βI, βII, and γ), novel or nonclassic PKCs (nPKCs; δ, ε, η, and θ), and atypical PKCs (ζ, ι and λ). Among PKC isozymes, PKCα is overexpressed or hyperactivated in several cancer cells or tissues (e.g., hepatoma, breast cancer, and melanoma) but has negligible activity in other normal tissues.[14-16]

We recently found a PKCα-specific substrate peptide that exhibited a higher phosphorylation ratio in tumor cells and tissues, compared with normal tissues.[17] Moreover, we have developed a novel tumor-targeted gene regulation system responding to PKCα by using the PKCα-specific substrate peptide. This system can distinguish between normal and tumor cells but is not tissue-specific.[18]

On the other hand, Kuroda's group reported the use of bionanocapsules (BNCs) as new drug and gene delivery carriers.[19,20] BNCs are hollow nanoparticles consisting of hepatitis B virus surface antigen molecules and a lipid bilayer. BNCs can be produced efficiently in recombinant yeast and are therefore free of other components of hepatitis B virus. The pre-S1 peptide displayed on BNCs specifically recognizes human hepatocytes.[19] Several studies have reported that BNCs showed high transfection efficiency and specificity to hepatocytes or hepatoma. The in vivo pinpoint delivery of genes and drugs to human hepatoma cells using BNCs has been demonstrated in mouse xenograft experiments.[19-21] Despite these advantages, however, BNCs are unable to distinguish between normal human hepatocytes and hepatoma cells.

In the present study we developed a novel hepatoma-targeted gene delivery system by combining our tumor cell–specific gene regulation system with human liver cell–specific BNCs. The complex showed increased transfection efficiency and selectivity for hepatoma cells, but no gene expression in normal human hepatocytes or human epidermoid tumor cells (A431).

Methods

Synthesis of polymers

For the synthesis of polymers, *N*-methacryloyl peptide (3.75 mg, 2.75 μmol), in which the methacryloyl group is attached at the N terminus of the peptide, *N*-isopropylacrylamide (20.4 mg, 180 μmol), and *N*-methacryloyl-polyethylene glycol (NPEG; 4.39 mg, molecular weight 12,000) were dissolved in degassed water and allowed to stand at room temperature for 1 hour after the addition of ammonium persulfate (3.1 mg, 2.9 mmol) and *N,N,N′,N′*-tetramethylethylenediamine (4 μL, 5.8 mmol) as the redox initiator couple. The product was then purified by overnight dialysis against water using a semipermeable membrane bag (with a molecular-weight cutoff of 100,000), followed by lyophilization, to produce a white powder. The positive polymer NPEG(S) contained serine at the phosphorylation site of the peptide, but this was substituted with alanine in the negative polymer, NPEG(A); the amino acid sequence of peptides is presented in Supplementary Figure 1 (available in the online version of this article).

Monitoring of phosphorylation of polymer-DNA complex by PKCα

Determination of phosphate incorporation into NPEG(S), NPEG(A), or peptides was carried out using a coupled-enzyme assay.[22] The oxidation of NADH (the reduced form of nicotinamide dinucleotide, or NAD^+), which can be monitored spectrophotometrically as an absorbance decrease at 340 nm, was coupled to the production of adenosine diphosphate using lactate dehydrogenase and pyruvate kinase. After incubation of the polymers and peptides (final peptide concentration was 32 μM) in 10 mM HEPES buffer (pH 7.2) containing 0.2 mM adenosine triphosphate (ATP), 10 mM $MgCl_2$, 1 mM phosphoenolpyruvate, 0.3 mM NADH, 10 U/μL lactate dehydrogenase, and 4 U/μL pyruvate kinase at 25°C, all reactions were initiated by the addition of activated PKCα.

Monitoring of disintegration of NPEG-DNA complex in response to PKCα

The disintegration of complexes in response to phosphorylation by PKCα was monitored by measuring the laser light scattering intensity of the complex dispersions using a Zetasizer (Malvern Instruments, Worcestershire, UK). The complex dispersions were diluted to obtain a measurement solution (15 μL) containing 25.6 nM peptide, 1 mM $MgCl_2$, 0.5 mM $CaCl_2$, 100 μM ATP, 2.0 mg/mL diacylglycerol, 2.5 μg/mL phosphatidylserine, 1 ng/mL PKCα, 10 mM HEPES (pH 7.3). The reaction was initiated by adding ATP and was performed at 25°C.

Transfection of NPEG-DNA-BNC complex into cells

The NPEG-DNA complex with various cation/anion (C/A) charge ratios (0.5, 1.0, and 2.0) was prepared by mixing NPEG with 0.5 μg of DNA for 10 minutes at room temperature and then for 5 minutes at 37°C. Next, 3 μL of liposome solution was prepared according to the recommended procedure (COATSOME EL-01-D; NOF Corporation, Tokyo, Japan), mixed with the polymer-DNA solution, and incubated at room temperature for 15 minutes. The NPEG-DNA-liposome solution was then mixed with 2.5 μg of BNCs for 15 minutes, and the resulting solution (NPEG-DNA-BNC complex) was added to cells. HuH-7 cells and normal human hepatocytes were maintained in Dulbecco's modified eagle's medium (Sigma, St. Louis, Missouri) supplemented with 10% (vol/vol) fetal bovine serum, penicillin (100 U/mL), streptomycin (100 μg/mL), and

amphotericin B (0.25 μg/mL) (all from Invitrogen, New York). The cells were kept in a humidified atmosphere containing 5% CO_2 and 95% air at 37°C. The medium was aspirated and changed 24 hours after addition of the complex. Fluorescence micrographs of the cells were obtained by microscopy (BZ-9000, Keyence Co., Osaka, Japan) 48 hours after transfection.

Quantification of DNA by real-time polymerase chain reaction

NPEG-DNA (pCMV-luc, 1.0 μg)-BNC complexes were prepared as described above, and the complex solution was poured onto the cells. At 24 hours after addition of the complex, medium was removed and the cells were washed three times with 300 μL phosphate-buffered saline. Extraction of DNA was performed according to the protocols for the High Pure PCR Template Preparation Kit (Roche Diagnostics GmbH, Mannheim, Germany). The levels of pCMV-luc in HuH-7 cells were estimated by quantitative real-time polymerase chain reaction (PCR) (LightCycler 1.5; Roche Diagnostics, Switzerland), in which a part of the luciferase region of pCMV-luc in extracted DNA samples was amplified by PCR. Sequences of PCR primers were as follows: forward, 5′-aagatggaaccgctgaga-3′ and reverse, 3′-cttctgccaaccgacg-5′. Each PCR reaction mixture (20 μL) consisted of 2 μL DNA template (1 ng/μL), 0.8 μL primers (10 μM stock solutions), and 10 μL SYBR Premix Ex Taq (TaKaRa Bio, Tokyo, Japan). The levels of pCMV-luc were standardized against total DNA amounts extracted from HuH-7 cells.

Cell viability assay

Cell viability was determined using WST-1 reagent {4-[3-(2-methoxy-4-nitrophenyl) -2-(4-nitrophenyl)-2H-5-tetrazolio]-1,3-benzene disulfonate sodium salt} (Dojindo Laboratories, Kumamoto, Japan). HuH-7 cells were incubated in the presence or absence of the NPEG-DNA-BNC complex (C/A = 0.5, 1.0, and 2.0) or Lipofectamine 2000 (10 μg/mL)-DNA complex for 24 hours in a 48-well plate. The conditioned medium in each well was replaced with 200 μL of fresh medium containing WST-1, and cells were incubated for 3 hours. The absorbance was measured at 450 nm. The percentage cell viability was calculated by normalizing the absorbance of treated cells to that of untreated cells. The results were analyzed statistically using two-sided Student's *t*-tests.

Animal experiments

Animal studies were performed in accordance with the Guidelines for Animal Experiments of Kyushu University. Male 5-week-old BALB/c nu/nu mice were used. Animals were inoculated subcutaneously with 1×10^7 tumor cells in 100 μL of Matrigel (BD Biosciences, Bedford, Massachusetts). Tumors were allowed to grow to a mean diameter of approximately 8 mm. NPEG-DNA-BNC complex containing 10 μg of DNA (C/A = 2.0) was prepared according to the method described above. A 140-μL aliquot of NPEG-DNA-BNC solution was injected directly into tumors or normal skin tissue. At 24 hours mice were anesthetized and injected intraperitoneally with 0.3 mL of 15 mg/mL D-luciferin (potassium salt; Promega, Wisconsin) in Ringer's solution. The images were obtained using a cooled C4742-98-26G02 charge-coupled device camera (Hamamatsu Photonics Systems, Hamamatsu, Japan) and analyzed for contrast and brightness using Adobe Photoshop 6.0 software. After a photographic image was taken, luminescent images were obtained from the anesthetized mice over the course of 10 minutes.

Results

Synthesis of polymers, NPEG(S) and NPEG(A)

We earlier had succeeded in inducing tumor-specific gene expression using a polymer composed of polyacrylamide as the main chain and PKCα-specific substrate peptide as the side chain.[18] In the present study the stability and size reduction of the complex was examined after the introduction of PEG units into the polymer as second side chains and the use of hydrophobic *N*-isopropylacrylamide as the main chain.[23,24] Two conjugates, NPEG(S) and its negative control NPEG(A), were designed using a similar procedure (Supplementary Figure 1, available in the online version of this article). NPEG(A) is not phosphorylated by PKCα, because the serine residue at the phosphorylation site is substituted with alanine. NPEG(S) and NPEG(A) contained the peptide side chain at a concentration of 0.9 and 1.2 mol%, respectively, and the PEG side chain at a concentration of 0.2 mol%, as estimated by the results of proton nuclear magnetic resonance and elemental analysis. The mean diameters of NPEG(S)-DNA and NPEG(A)-DNA were <100 nm at all C/A ratios (Supplementary Table 1, available in the online version of this article).

Disintegration of NPEG-DNA complex by the addition of PKCα

We investigated if NPEG(S) could act as a substrate of PKCα using a coupled-enzyme assay.[22] In this assay the production of adenosine diphosphate, which is derived from ATP as a byproduct of the peptide phosphorylation, brings about the oxidation of NADH using lactate dehydrogenase and pyruvate kinase. Phosphorylation can thus be monitored by the reduction in absorbance at 340 nm. A time-dependent reduction in the absorbance at 340 nm was identified after the addition of PKCα (Figure 1, *A*). A reduction in absorbance at 340 nm was observed in both peptide(S) and NPEG(S)-DNA, but the absorbance remained constant in the case of peptide(A) and NPEG(A)-DNA. These results suggest that the peptide grafted in the NPEG polymer is phosphorylated by PKCα after being incorporated into the polymer backbone and combined with DNA.

We monitored the disintegration of the NPEG(S)-DNA complex using the laser light scattering intensity. The time-dependent change in the intensity is presented in Figure 1, *B*. After the addition of PKCα, the intensity of NPEG(S)-DNA gradually decreased, whereas no change was detected in NPEG(A)-DNA. These results indicate that the NPEG(S)-DNA complex can be disintegrated by phosphorylation of the peptide.

Cytotoxicity of NPEG-DNA-BNC

Recently, Kuroda's group succeeded in combining large materials (100-nm fluorescence-labeled polystyrene beads and >30–kilobase pair plasmids) with BNCs using a liposome

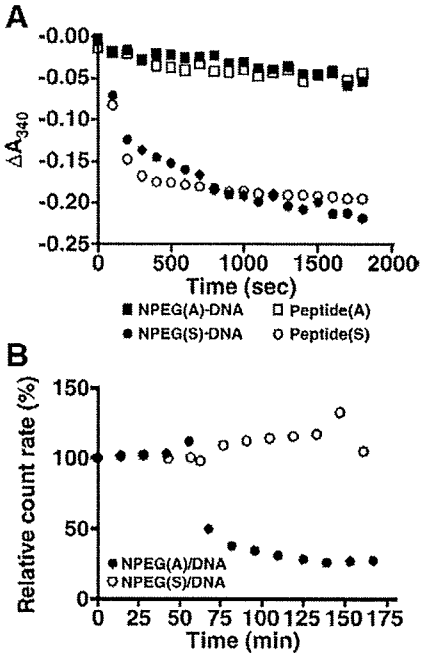

Figure 1. **(A)** Monitoring of phosphorylation of grafted peptide in the form of a NPEG-DNA complex or substrate peptide, using a coupled enzyme assay. The enzymatic reaction was started at 0 minutes by adding adenosine triphosphate. The charge ratio of the complex was 2.0. **(B)** Change of relative scattering intensity of NPEG-DNA complex dispersions after initiation of enzymatic reaction with protein kinase Cα (PKCα).

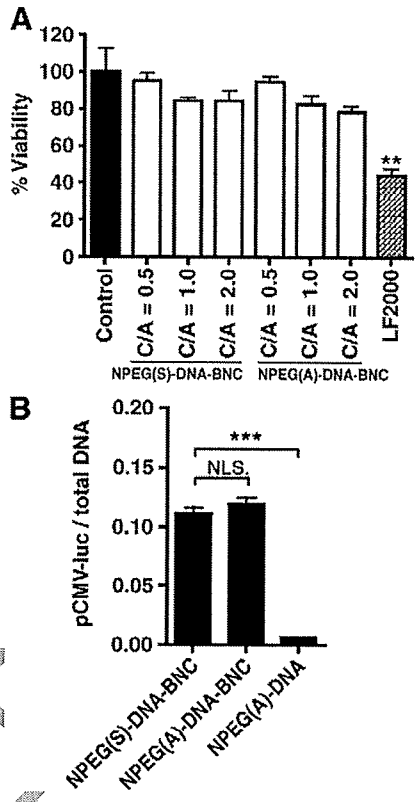

Figure 2. **(A)** Cytotoxicity of NPEG-DNA-BNC (charge ratio, C/A = 0.5, 1.0, and 2.0) or Lipofectamine 2000–DNA complexes toward cells. Cells were incubated for 24 hours in a 48-well plate, and cell viability was determined by WST-1 assay. The cell viability (%) was calculated by normalizing the absorbance of treated cells to that of untreated control cells. Error bars represent standard errors of the means of three experiments. Control sample (no treated cells) showed significantly higher cell viability compared with cells treated with Lipofectamine 2000 (**$P < .05$). **(B)** Quantification of DNA by real-time polymerase chain reaction. Cells were incubated with NPEG-DNA complexes with or without bionanocapsules (BNC) for 24 hours. Error bars represent standard errors of the means of three experiments. ***$P < .001$.

composed of dioleoylphosphatidylethanolamine/cholesterol–DC-6-14.[20] In the present study we used the same liposome to form the NPEG-DNA complex with BNCs. BNCs are nanoparticles composed of human hepatocyte L protein embedded in a yeast endoplasmic reticulum membrane–derived phospholipid vesicle, and it is therefore able to combine effectively with the NPEG-DNA complex coated by a phospholipid liposome vesicle.[20]

The cytotoxicity of NPEG-DNA-BNC was determined using the WST-1 assay. The NPEG-DNA-BNC complexes showed no toxicity to cells at C/A ratios of 0.5, 1.0, and 2.0, whereas the commercial transfection reagent (Lipofectamine 2000) showed significant cytotoxicity (Figure 2, *A*).

Quantification of DNA by real-time PCR

To investigate the transfection ability of the NPEG-DNA-BNC complex into hepatoma cells, the amounts of DNA after transfection were quantified. Cells were lysed and the amount of DNA was quantified by real-time PCR. The level of DNA transferred by NPEG(S) and BNCs was significantly higher than that by NPEG(S) alone ($P < .001$) (Figure 2, *B*). However, the level of DNA transferred by NPEG(S)-DNA-BNC was similar to that by NPEG(A)-DNA-BNC. These results show that the delivery of NPEG-DNA into cells was promoted by BNCs. No difference in the delivery into cells between NPEG(A) and NPEG(S) means that NPEG(A) can be used as a negative control.

Delivery of NPEG–green fluorescent protein–encoding DNA-BNC into HuH-7 cells or normal human hepatocytes

We determined if phosphorylation by PKCα was able to induce gene expression from the NPEG(S)-DNA-BNC complex after transfection. HuH-7 cells were treated with NPEG(S)-GFP gene–BNC, and GFP expression was examined. GFP expression was observed at all C/A ratios (0.5-2.0) of NPEG(S)-DNA-BNC, whereas no GFP expression was found at a C/A ratio of 2.0 in the case of NPEG(A)-DNA-BNC (Figure 3).

Our developed gene delivery system needed to show hepatoma-specific gene delivery, and no gene expression in normal hepatocytes. Thus, we transfected the NPEG-DNA-BNC complex into normal human hepatocytes. GFP expression was observed in the DNA-BNC–transfected cells (Figure 3), whereas no expression occurred after transfection of DNA alone (data not shown), indicating that the BNCs had normal gene transfection ability into human hepatocytes. However,

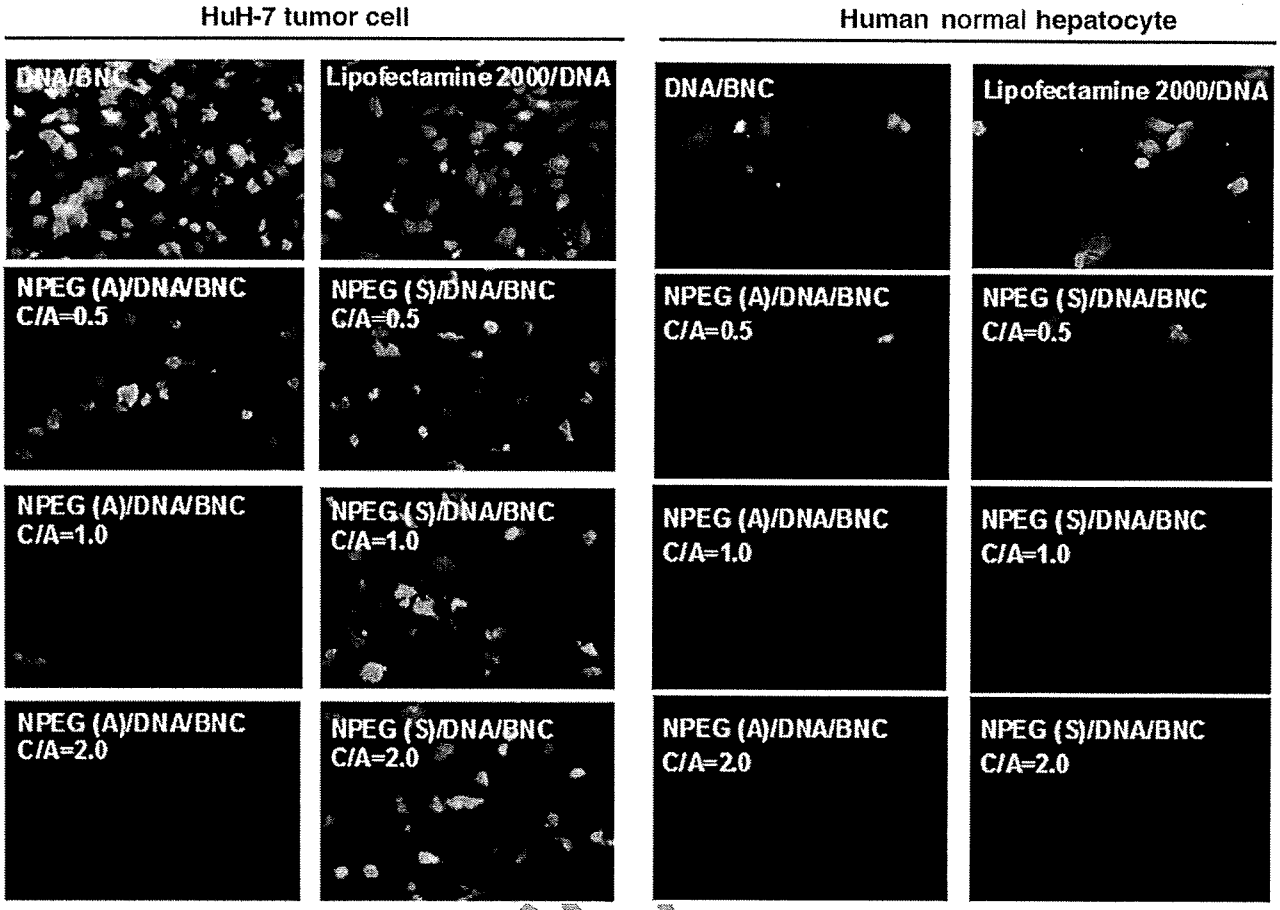

Figure 3. Green fluorescent protein (GFP) expression after transfection of NPEG–GFP-encoding DNA–BNC complex into normal human hepatocytes or HuH-7 tumor cells. C/A, charge ratio.

GFP expression was depressed completely when the NPEG(S)-DNA-BNC complex at a C/A ratio of 2.0 was transfected into normal human hepatocytes.

At C/A ratios of 0.5 and 1.0, however, gene expression was identified in NPEG(A)-DNA-BNC complex–transfected cells, which may be related to the instability of the complex.

Delivery of NPEG–luciferase-encoding DNA–BNC complex into xenografted mice

On the basis of the results of the in vitro experiments, we applied our system in mice xenografted with tumors at a C/A ratio of 2.0. NPEG–luciferase gene–BNC complexes were injected directly into HuH-7 tumors or normal skin tissue of mice. Tumor-specific luciferase expression was observed with NPEG(S)-DNA-BNC. On the other hand, no expression was found in either tumor or normal tissue after injection of the negative control (NPEG(A)-DNA-BNC) (Figure 4).

The hepatoma specificity of the NPEG-DNA-BNC system was tested by applying it to human epidermoid tumor tissues (A431) containing activated PKCα. No gene expression was detected from A431 tumor tissues, indicating that the NPEG-DNA-BNC complex is a useful system for hepatoma-selective gene expression.

Discussion

Hepatoma-targeted therapy is an important means of increasing treatment efficiency and avoiding undesirable side effects. Intracellular signals have recently been investigated as therapeutic targets for hepatomas. This therapeutic approach involves the use of inhibitors to target specific protein kinases. Hepatoma cells make use of two main signal transduction pathways for tumor cell differentiation, proliferation, and survival; the RAS/RAF/MEK/ERK and the PI3K/Akt/mTOR pathways.[4,6-8,25] Their various pharmacological inhibitors, such as sorafenib and sunitinib, have been tested extensively in preclinical and early-stage clinical trials for the treatment of hepatoma. These inhibitors have been shown to inhibit the promotion, as well as the proliferation, of hepatomas, but have poor specificity for hepatoma cells.[4,6-8,26] Moreover, inhibitors of PKC isozymes (e.g., staurosporin, tamoxifen, and UCN-01), including PKCα, that are activated by the RAS/RAF/MEK/ERK and the PI3K/Akt pathways, show low specificity for hepatoma cells, and because these signals are involved in normal cells, their suppression by inhibitors leads to the development of undesirable side effects.[13-16] These results indicate the limitations associated with hepatoma cell–specific treatment using inhibitors of intracellular signals.[4,6-8,13-16,26]

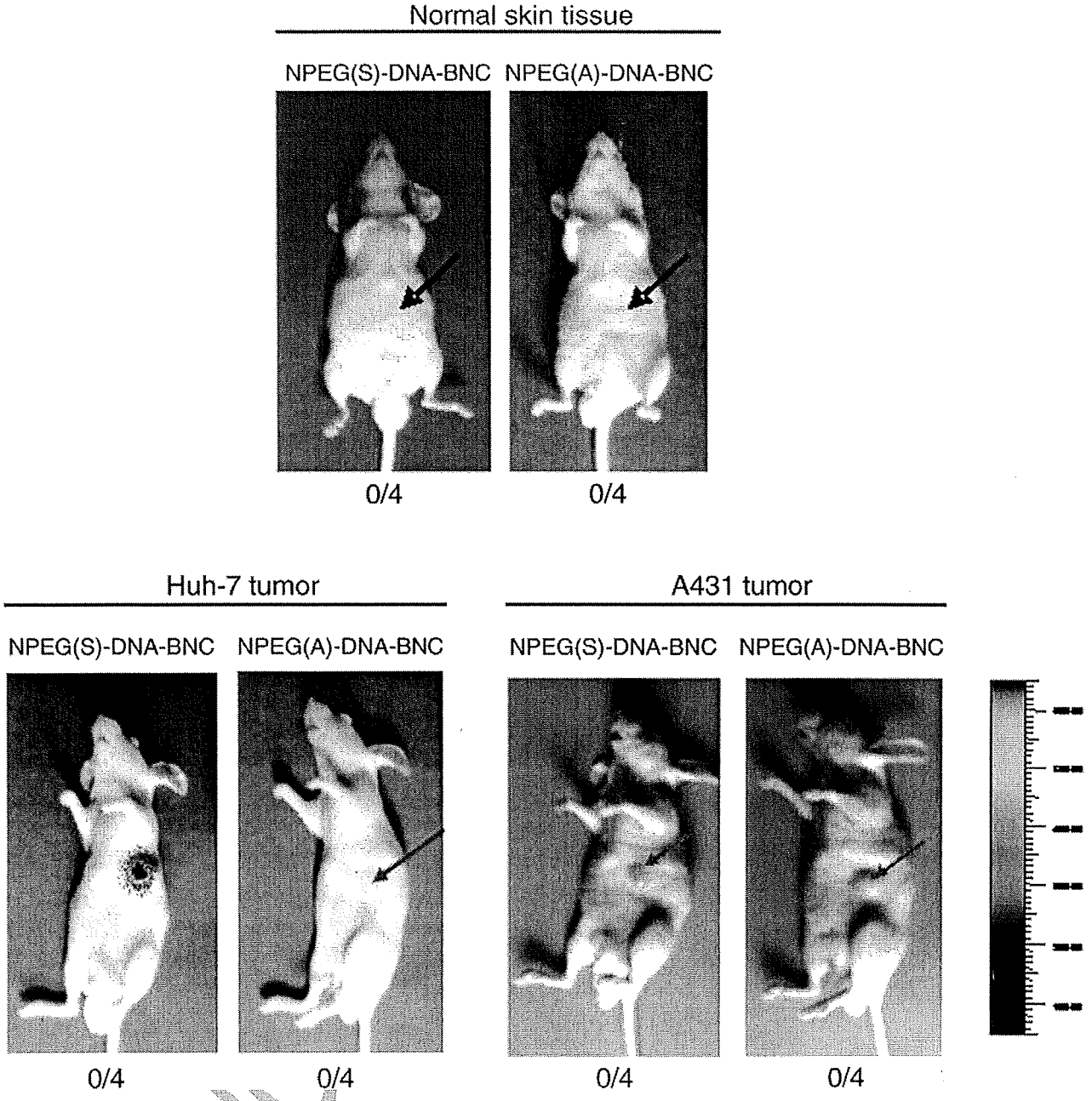

Figure 4. Luciferase activity in normal subcutaneous, xenografted HuH-7 tumors or A431 tumors 24 hours after direct injection of NPEG-DNA-BNC complexes (C/A = 2.0). Numbers of luciferase-expressing mice per total number of mice are described below the pictures. Arrows indicate the injection site of NPEG-DNA-BNC complexes.

In this study we developed a novel system for hepatoma-specific therapy using the combination of a tumor cell–specific gene regulation system responding to PKCα, and human hepatocyte-specific BNCs. In this system, hydrophilic polymers grafted with a cationic PKCα-specific substrate peptide, form complexes with DNA. DNA transcription is repressed when it forms a complex with the polymer, as a result of steric hindrance. The grafted cationic peptides act as substrates for the target PKCα, which is activated specifically in hepatoma cells. Phosphorylation by PKCα reduces the peptide cationic charge, resulting in release of DNA from the complex. Thus, the process of gene expression involves (1) the strong binding of complexes to the surface of hepatoma cells by BNCs, (2) the transfection of complexes into the cytosol by endocytosis, and then (3) DNA release from the NPEG-DNA complex by phosphorylation of the substrate peptide by PKCα. The NPEG-DNA-BNC complex showed no cytotoxicity to cells at all C/A ratios (0.5, 1.0, and 2.0) (Figure 2, *A*). Our system demonstrated hepatoma-specific gene expression both in vitro and in vivo. Interestingly, GFP expression was identified in the NPEG(S)-DNA-BNC complex–transfected hepatoma cells (C/A = 2.0), but no expression was detected in complex-transfected normal human hepatocytes (Figure 3). These results

demonstrate that this gene delivery system can distinguish between hepatoma cells and normal hepatocytes. Moreover, using mice xenografted with human tumors, we identified gene expression from hepatoma HuH-7 tumors but not from A431 tumors (Figure 4) or human lung adenocarcinomas (A549) (data not shown), indicating hepatoma-selective expression. Overexpression of PKCα has already been detected in these three types of tumor cells.[18] Based on these results, our novel gene regulation system has great potential for applications in hepatoma-specific gene therapy and molecular imaging.

Appendix A. Supplementary Material

Supplementary data associated with this article can be found, in the online version, at doi:10.1016/j.nano.2010.01.007.

References

1. Berrino F, De Angelis R, Sant M, Rosso S, Lasota M, Coebergh JW, et al. Survival for eight major cancers and all cancers combined for European adults diagnosed in 1995-99: resutls of the EUROCARE-4 study. Lancet Oncol 2007;8:773-83.
2. Jemal A, Siegel R, Ward E, Murray T, Xu J, Thun MJ. Cancer statistics, 2007. CA Cancer J Clin 2007;57:43-66.
3. Yu AS, Keeffe EB. Management of hepatocellular carcinoma. Rev Gastroenterol Disord 2003;3:8-24.
4. Llovet JM, Bruix J. Molecular targeted therapies in hepatocellular carcinoma. Hepatology 2008;48:1312-27.
5. Herr I, Schemmer P, Büchler MW. On the TRAIL to therapeutic intervention in liver disease. Hepatology 2008;46:266-74.
6. Hui KM. Current approaches in the transcriptional-guided gene therapy of human hepatocellular carcinoma. Curr Opin Mol Ther 2007;9:378-84.
7. Avila MA, Berasain C, Sangro B, Prieto J. New therapies for hepatocellular carcinoma. Oncogene 2006;25:3866-84.
8. Calvisi DF, Pascale RM, Feo F. Dissection of signal transduction pathways as a tool for the development of targeted therapies of hepatocellular carcinoma. Rev Recent Clin Trials 2007;2:217-36.
9. Riki T, Kang JH, Kim JH, Tomiyama T, Mori T, Niidome T, et al. Protein kinase Cα-specific peptide substrate graft-type copolymer for cancer cell-specific gene regulation systems. J Control Release 2009;139:133-9.
10. Kawamura K, Oishi J, Kang JH, Kodama K, Sonoda T, Murata M, et al. Intracellular signal-responsive gene carrier for cell-specific gene expression. Biomacromolecules 2005;6:908-13.
11. Oishi J, Kawamura K, Kang JH, Kodama K, Sonoda T, Murata M, et al. An intracellular kinase signal-responsible gene-carrier for cell specific gene therapy. J Control Release 2006;110:431-6.
12. Manning G, Whyte DB, Martinez R, Hunter T, Sudarsanam S. The protein kinase complement of the human genome. Science 2002;298: 1912-34.
13. Cohen P. Protein kinases—the major drug targets of the twenty-first century? Nat Rev Drug Discov 2002;1:309-15.
14. Hofmann J. Protein kinase C isozymes as potential targets for anticancer therapy. Curr Cancer Drug Targets 2004;4:125-46.
15. Goekjian PG, Jirousek MR. Protein kinase C inhibitors as novel anticancer drugs. Expert Opin Investig Drugs 2001;10:2117-40.
16. O'Brian CA, Chu F, Bornmann WG, Maxwell DS. Protein kinase Cα and ε small-molecule targeted therapeutics: a new roadmap to two holy grails in drug discovery? Expert Rev Anticancer Ther 2006;6:175-86.
17. Kang JH, Asai D, Yamada S, Toita R, Oishi J, Mori T, et al. A short peptide is a protein kinase C (PKC) α-specific substrate. Proteomics 2008;8:2006-11.
18. Kang JH, Asai D, Kim JH, Mori T, Toita R, Tomiyama T, et al. Design of polymer carriers for cancer-specific gene targeting: utilization of abnormal protein kinase Cα activation in cancer cells. J Am Chem Soc 2008;130:14906-7.
19. Yamada T, Iwasaki Y, Tada H, Iwabuki H, Chuah MKL, Vanden-Driessche T, et al. Nanoparticles for the delivery of genes and drugs to human hepatocytes. Nat Biotechnol 2003;21:885-90.
20. Jung J, Tatematsu K, Matsuzaki T, Okajima T, Ueda M, Kondo A, et al. Bio-nanocapsule conjugated with liposomes for in vivo pinpoint delivery of various materials. J Control Release 2008;125:255-64.
21. Kasuya T, Jung J, Kadoya H, Matsuzaki T, Tatematshu K, Okajima T, et al. In vivo delivery of bionanocapsules displaying *Phaseolus vulgaris* agglutinin-L4 isolectin to malignant tumors overexpressing *N*-acetylglucosaminyltransferase V. Hum Gene Ther 2008;19:887-95.
22. Cook PF, Neville ME, Vrana KE, Hartl FT, Roskoski R. Adenosine cyclic 3′,5′-monophosphate dependent protein kinase: kinetic mechanism for the bovine skeletal muscle catalytic subunit. Biochemistry 1982;21:5794-9.
23. Kumar TR, Soppimath K, Nachaegari SK. Novel delivery technologies for protein and peptide therapeutics. Curr Pharm Biotechnol 2006;7: 261-76.
24. Jeong B, Kim SW, Bae YH. Thermosensitive sol-gel reversible hydrogels. Adv Drug Deliv Rev 2002;54:37-51.
25. Boyault S, Rickman D, de Reynies A, Balabaud C, Rebouissou S, Jeannot E, et al. Transcriptome classification of HCC is related to gene alterations and new therapeutic targets. Hepatology 2007;45:42-52.
26. Tommasi S, Pinto R, Pilato B, Paradiso A. Molecular pathways and related target therapies in liver carcinoma. Curr Pharm Des 2007;13: 3279-87.

AUTHOR QUERY FORM

ELSEVIER	**Journal: NANO** **Article Number: 335**	**Please e-mail or fax your responses and any corrections to:** **Angela Stafford** **E-mail: stafforda@cadmus.com** **Tel: 717-738-9335** **Fax: 717-738-9479 or 717-738-9478**

Dear Author,

Any queries or remarks that have arisen during the processing of your manuscript are listed below and highlighted by flags in the proof. Please check your proof carefully and mark all corrections at the appropriate place in the proof (e.g., by using on-screen annotation in the PDF file) or compile them in a separate list.

For correction or revision of any artwork, please consult http://www.elsevier.com/artworkinstructions.

Articles in Special Issues: Please ensure that the words 'this issue' are added (in the list and text) to any references to other articles in this Special Issue.

Uncited references: References that occur in the reference list but not in the text – please position each reference in the text or delete it from the list.
Missing references: References listed below were noted in the text but are missing from the reference list – please make the list complete or remove the references from the text.

Location in article	Query / remark Please insert your reply or correction at the corresponding line in the proof
Q1	Please check refs 19, 20. Kuroda's name not shown.
Q2	Okay to add NPEG here, because this is where you define it? See also figure legends.
Q3	Please supply a temperature range for "room temperature."
Q4	Please provide city in New York state where Invitrogen is located.
Q5	Please provide city in Switzerland where Roche Diagnostics (supplier of LightCycler 1.5) is located.
Q6	Please supply the manufacturer and location (city and state if in the US, or city and country, if outside of the US) for Lipofectamine 2000.
Q7	Pls define NPEG, Peptide(S), and Peptide(A).
Q8	Please clarify what is meant by the (A) and (S) in peptide(A) and peptide(S).
Q9	Please clarify what is meant by the (A) and (S) in peptide(A) and peptide(S).
Q10	Please check refs 19, 20. Kuroda's name not shown.
Q11	Okay to change WST to WST-1 as before?
Q12	Please supply the manufacturer for Lipofectamine 2000.

Electronic file usage
Sometimes we are unable to process the electronic file of your article and/or artwork. If this is the case, we have proceeded by:

Biochemical and Biophysical Research Communications 393 (2010) 55–60

Contents lists available at ScienceDirect

Biochemical and Biophysical Research Communications

journal homepage: www.elsevier.com/locate/ybbrc

Identification of genes related to heart failure using global gene expression profiling of human failing myocardium

Kyung-Duk Min [a], Masanori Asakura [a,*], Yulin Liao [c], Kenji Nakamaru [d], Hidetoshi Okazaki [a], Tomoko Takahashi [d], Kazunori Fujimoto [d], Shin Ito [a], Ayako Takahashi [a], Hiroshi Asanuma [e], Satoru Yamazaki [b], Tetsuo Minamino [g], Shoji Sanada [a], Osamu Seguchi [a], Atsushi Nakano [a], Yosuke Ando [d], Toshiaki Otsuka [d], Hidehiko Furukawa [d], Tadashi Isomura [f], Seiji Takashima [g], Naoki Mochizuki [b], Masafumi Kitakaze [a]

[a] Department of Cardiovascular Medicine, Osaka, Japan
[b] Research Institute, National Cardiovascular Center, Osaka, Japan
[c] Department of Pathophysiology, Southern Medical University, Guangzhou 510515, China
[d] R&D Division, Daiichi Sankyo Co., Ltd., Tokyo, Japan
[e] Department of Emergency Room Medicine, Kinki University School of Medicine, Sayama, Osaka, Japan
[f] Hayama Heart Center, Hayama, Kanagawa, Japan
[g] Department of Cardiovascular Medicine, Osaka University Graduate School of Medicine, Suita, Osaka, Japan

ARTICLE INFO

Article history:
Received 12 January 2010
Available online 25 January 2010

Keywords:
Gene expression
cDNA microarray
Heart failure
Clinical parameter

ABSTRACT

Although various management methods have been developed for heart failure, it is necessary to investigate the diagnostic or therapeutic targets of heart failure. Accordingly, we have developed different approaches for managing heart failure by using conventional microarray analyses. We analyzed gene expression profiles of myocardial samples from 12 patients with heart failure and constructed datasets of heart failure-associated genes using clinical parameters such as pulmonary artery pressure (PAP) and ejection fraction (EF). From these 12 genes, we selected four genes with high expression levels in the heart, and examined their novelty by performing a literature-based search. In addition, we included four G-protein-coupled receptor (GPCR)-encoding genes, three enzyme-encoding genes, and one ion-channel protein-encoding gene to identify a drug target for heart failure using *in silico* microarray database. After the *in vitro* functional screening using adenovirus transfections of 12 genes into rat cardiomyocytes, we generated gene-targeting mice of five candidate genes, namely, *MYLK3*, *GPR37L1*, *GPR35*, *MMP23*, and *NBC1*. The results revealed that systolic blood pressure differed significantly between *GPR35*-KO and *GPR35*-WT mice as well as between *GPR37L1*-Tg and *GPR37L1*-KO mice. Further, the heart weight/body weight ratio between *MYLK3*-Tg and *MYLK3*-WT mice and between *GPR37L1*-Tg and *GPR37L1*-KO mice differed significantly. Hence, microarray analysis combined with clinical parameters can be an effective method to identify novel therapeutic targets for the prevention or management of heart failure.

Introduction

Heart failure is a multi-factorial condition with increasing prevalence worldwide; further, a significant increase has been observed in the mortality rate and economic impact associated with this condition. In the last 20 years, substantial development of treatment for heart failure, including angiotensin-converting-enzyme inhibitors [1] and beta-blockers [2,3], has greatly improved the prognosis of the patients with heart failure. However, despite these rapid advancements in the management of heart failure, effective treatment of end-stage heart failure without providing ventricular assistance or heart transplantation is still difficult. Investigation of new and unexplored targets for the prevention or treatment of heart failure is warranted. Global gene expression analysis using microarray technique has been used in the last decade to identify biomarkers or drug targets for heart failure [4–10]. Several gene expression signatures of heart failure have been identified by analyzing independent microarray datasets [11,12]. However, most of these analyses did not consider the severity of heart failure. Because the severity of heart failure may quantitatively reflect the expression levels of genes such as the natriuretic

* Corresponding author. Address: Department of Research and Development of Clinical Research, National Cardiovascular Center, 5-7-1 Fujishirodai, Suita, Osaka 565-8565, Japan.
E-mail address: masakura@hsp.ncvc.go.jp (M. Asakura).

0006-291X/$ - see front matter © 2010 Elsevier Inc. All rights reserved.
doi:10.1016/j.bbrc.2010.01.076

peptide-encoding gene, expression analysis combined with the severity of heart failure could be an appropriate method to identify heart failure-related genes. However, microarray analysis of genes expressed in failing myocardium while considering the severity of heart failure has not yet been reported.

Hence, we investigated the genes whose expression level correlated with clinical parameters such as pulmonary artery pressure (PAP), left ventricular ejection fraction (EF), and brain natriuretic peptide (BNP) mRNA level. Using this approach, we identified cardiac myosin light chain kinase as a novel heart failure-related gene [13]. Here, we describe newly identified several genes whose expression correlated with clinical parameters and additional genes encoding G-protein-coupled receptor genes (GPCRs), other enzymes and ion-channel proteins, and performed the functional analysis of these heart failure-related genes. This novel strategy involving the use of clinical parameters might find potential applications for the identification of disease-associated genes that could not be detected using conventional microarray techniques.

Materials and methods

Patient characteristics. We recruited 12 patients (11 males and 1 female) with heart failure and obtained written informed consent from them. The patients were diagnosed with severe chronic heart failure due to various cardiac diseases such as dilated cardiomyopathy and myocardial infarction [13]. The average age of patients was 55 ± 13 years. The plasma level of BNP, which is the best marker for the severity of heart failure, ranged from 80 to 2710 pg/ml. The mean PAP measured using a Swan-Ganz catheter 1–4 weeks before the operation varied between 16 and 59 mmHg. The average of EF determined by echocardiography on the day before the operation was 32.5% ± 12.4%.

Microarray analysis and subsequent in silico functional analysis. RNA was extracted from myocardium samples of 12 heart failure patients who had undergone either Batista or Dor surgeries. RNA samples of non-failing hearts were purchased from Biochain, Inc. Complementary RNA (cRNA) was prepared from RNA samples and hybridized to HG-U95 Affymetrix GeneChip (Affymetrix, US). The expression data were analyzed using Microarray Analysis Suite version 5.0 software. Among all the genes detected on the microarray, we selected the genes whose expression was significantly different in the failing and non-failing myocardial samples ($p < 0.005$). From these genes, we selected genes whose expression was correlated with PAP, EF, and BNP mRNA level, with 0.7 being the cutoff value of the correlation coefficient. The values of PAP, EF, and BNP mRNA level used for the correlation analysis were normalized to their median during the measurements. Subsequently, the functional analysis of datasets was performed using Ingenuity Pathway Analysis (Ingenuity® Systems; www.ingenuity.com), and the biological functions most significant to the dataset were identified.

Cell culture. Cardiomyocytes were harvested before the experiments from 2- to 3-day-old neonatal rats and cultured as described in previous studies [14]. Briefly, primary cardiomyocytes isolated from neonatal rats were grown in Dulbecco's modified Eagle medium/F12 (Gibco) supplemented with 10% fetal calf serum for 72 h, and then cultured in a serum-free condition for 24 h.

Adenovirus generation and transfection. Adenovirus constructs encoding the genes of interest were generated using the ViraPower Adenoviral Expression System (Invitrogen, US) according to the manufacturer's method. Adenovirus vectors were transfected to cultured cardiomyocytes for 12 h according to the published protocol.

In vitro functional analysis of genes. Cultured rat cardiomyocytes were infected by adenovirus vectors. After 24 h, hypertrophic reaction, cell viability, and cellular morphology were assessed. Hypertrophic reaction was determined by estimating the incorporation of [^{3}H]phenylalanine. In brief, [^{3}H]phenylalanine was added to the culture medium at the final concentration of 0.1 μCi/ml, and the cells were incubated for an additional 24 h. Then, the incorporation of [^{3}H]phenylalanine was determined by counting the radioactivity of each sample with a liquid scintillation counter. The viability of cardiomyocytes was evaluated by the Alamar blue assay according to the manufacturer's method. The morphology of cardiomyocytes was evaluated 24 h after adenovirus transfections.

Generation of transgenic and knockout mice. To generate transgenic mice, open reading frame of each gene, namely, *Mylk3*, *Gpr37l1*, or *Nbc1* was amplified from mouse cDNA by PCR, with Sal I site linker on each end, and cloned into Sal I site of alpha-MHC clone 26 vector. Then the DNAs used in the microinjections were released from the vector by digestion with NotI and were microinjected into fertilized eggs of mouse. Founder mice were identified by PCR analysis with appropriate primers. To develop *Gpr37l1* knockout mice, the targeting vector was assembled to replace the exon 1 and 2 by neomycin selection cassete resulting in the absence of *Gpr37l1* protein. W9.5 ES cells were electroporated with linearized targeting vector. ES cell clones with successful homologous recombination was determined by the PCR and subsequent direct sequence. From these targeted ES cells, the chimera mice were bred to C57 BL/6 females to generated F1 and F2 offsprings were obtained. The *Gpr37l1* null mice were determined by PCR genotyping of F2 offsprings. The knockout mice of *Gpr35* and *Mmp23* (*the* mouse ortholog of MMP23B) were purchased from Deltagen, Inc. (California, US).

Invasive blood pressure measurement. The phenotype of the gene-targeted mice was examined. Before sacrificing the mice, their hemodynamic parameters were evaluated. The mice were anesthetized and ventilated, and a Millar catheter was inserted via right carotid artery. The left-ventricular systolic and end-diastolic pressures were measured. Then, the mice were sacrificed and the weight of the whole body and heart was determined.

Statistical analysis. Unpaired Student's *t*-test was used for comparing the two groups. Results are expressed as means ± SEM, and *p* value less than 0.05 was considered statistically significant.

Results

Identification of heart failure-related genes by expression analysis using clinical parameters

We performed microarray analysis of the genes expressed in failing myocardium obtained from 12 patients with heart failure and the genes expressed in non-failing myocardium from two normal objects whose characteristics were reported in the previous study [13]. Although all patients were diagnosed with chronic heart failure, the plasma BNP level, which is an index of the severity of heart failure, ranged from 80 to 2710 pg/ml, suggesting that the severity of heart failure varied extensively among the patients. This marked difference in the severity of heart failure reflects the fact that the gene expression patterns in the 12 patients were not uniform, as shown in Fig. 1A. Thus, we analyzed gene expression profiles of failing myocardium using clinical parameters representing the severity of heart failure. We identified 166 and 194 genes whose expressions were correlated with PAP and BNP mRNA level, respectively (Fig. 1B and Supplementary Tables S1, S2). Among these, 49 genes correlated with both PAP and BNP mRNA level (Fig. 1C). The expression of only two genes, namely, *FMO2* and *LMAN1L*, correlated with the EF. We investigated the functional categories of these genes by performing Ingenuity Pathway Analysis. The number of genes in each group, functional categories, and

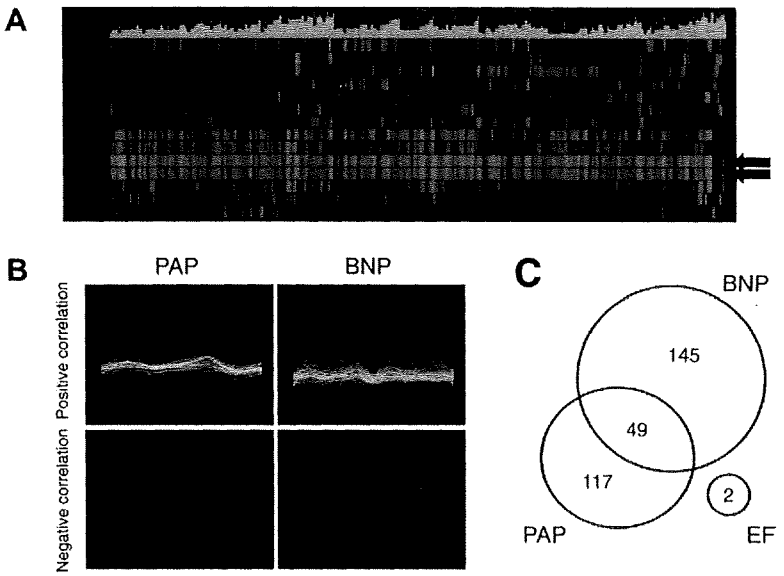

Fig. 1. The gene expression profile of human failing or non-failing myocardium. Gene expression levels of myocardial samples from 12 patients with severe heart failure and from two normals were analyzed using microarray. (A) Heat maps showing the genes with differential expression between the 12 failing myocardial samples and the two non-failing myocardial samples. Red color indicates upregulated gene expression. Green color indicates downregulated gene expression. Arrows indicate non-failing samples. (B) Expression profile of positively or negatively correlated genes to pulmonary artery pressure (PAP) or brain natriuretic peptide (BNP) mRNA level ($r > 0.7$). (C) Venn diagram of genes correlated with PAP, BNP, and ejection fraction.

Table 1
Datasets of genes whose expressions were correlated to clinical parameters.

	PAP	EF	BNP mRNA level
Positive correlation			
Number	124	1	175
Function	Cardiovascular system development and function Cell death	–	Cardiovascular system development and function Cell cycle
Representative genes	*ARNT, MYOCD, SMARCA4* *BGN, CFLAR, EEF2, MTPN*	*LMAN1L*	*BTG1, NPPA, NPPB, SERPNF1* *CKS1B, DDR2, FCGR2B, FN1*
Negative correlation			
Number	42	1	19
Function	Skeletal and muscular system development and function Cellular assembly and organization	–	Skeletal and muscular system development and function Cellular assembly and organization
Representative genes	*PIK3R1, PRKAR1A, SLMAP* *C19ORF20, RAB9A, SYNGAP1, TTN*	*FMO2*	*ACTC1, RBBP4, TTN*

The function of gene sets was analyzed by Ingenuity Pathway Analysis.
PAP, pulmonary artery pressure; EF, ejection fraction; BNP, brain natriuretic peptide.

representative genes are shown in Table 1. Interestingly, both gene sets correlated positively with PAP and BNP mRNA level were most associated with the same functional category of "cardiovascular system development and function", although the included genes were different. Similarly, the gene sets correlated negatively with both PAP and BNP mRNA level had most association with common functional categories of "skeletal and muscular system development and function" and "cellular assembly and organization".

Selection of 12 genes for in vitro screening

Among the genes selected using clinical parameters, we selected those genes that showed high expression levels in the heart by performing microarray analysis. On the basis of their novelty determined by a literature-based search, we selected four genes for further investigation (Table 2). Concurrently, to identify possible drug targets, we included four orphan GPCRs and four additional genes (three enzyme-encoding genes and one ion-channel protein-encoding gene) in the further analysis. The *RHOQ* and *STK38* genes were selected based on their correlation with BNP mRNA level and PAP, respectively. *GPR161* and *NBC1* were selected owing to their high expression level in the heart. *GPR37L1, GPR35, F2RL2*, and *MMP23B* were selected because of their high expression level in the heart, and their association with the cardiac diseases-related genes listed in the database was determined by *in silico* analysis.

Functional analysis of genes on the basis of adenovirus-mediated overexpression of proteins in neonatal rat cardiomyocytes

To determine which of the selected genes were associated with the physiological functions of the heart, we first generated adenovirus vectors for each gene listed in Table 2 and transfected these vectors into neonatal rat cardiomyocytes. Next, we evaluated the hypertrophic reaction, viability, and morphology of the transfected cardiomyocytes. Among the 12 selected genes, three adenovirus-mediated genes decreased the incorporation of [^{3}H]phenylalanine in neonatal rat cardiomyocytes (Table 2); the expression of one

Table 2
In vitro functional screening of the 12 candidate genes.

Probe set ID	Gene symbol	Gene name	Criteria for selection	*p* value	[^{3}H]PA intake	Fluorescence of Alamar blue	Cellular morphology
Genes relevant to clinical parameters							
75678_at	*MYLK3*	Myosin light chain kinase 3	Correlation with PAP ($r = 0.792$)	0.00262	No change	No change	Spiking
49333_at	*XPR1*	Xenotropic and polytropic retrovirus receptor	Correlation with PAP ($r = 0.765$), GPCR, change in CHF	0.00045	No change	No change	No change
38435_at	*PRDX4*	Peroxiredoxin 4	Correlation with BNP ($r = 0.863$)	0.00024	Increased	Decreased	No change
45314_at	*SMOC2*	SPARC related modular calcium binding 2	Correlation with both PAP and BNP ($r = 0.715$ and 0.758, respectively)	0.00444	No change	No change	No change
Genes encoding orphan GPCRs							
35544_at	*GPR37L1*	G-protein-coupled receptor 37 like 1	Orphan GPCR, downregulated in CVD	>0.005	Decreased	Decreased	Apoptosis
31700_at	*GPR35*	G-protein-coupled receptor 35	Orphan GPCR, upregulated in MI	0.00216	Decreased	Decreased	Hypertrophy
45204_at	*F2RL2*	Coagulation factor II (thrombin) receptor-like 2	GPCR, change in CVD	>0.005	Increased	No change	No change
40299_at	*GPR161*	G-protein-coupled receptor 161	GPCR, expression in heart	>0.005	Decreased	Decreased	No change
Genes encoding interesting enzymes or ion-channels							
38950_at	*MMP23B*	Matrix metallopeptidase 23B	Family of MMP, change in CHF	>0.005	No change	Decreased	No change
35285_at	*NBC1*	Na^+–HCO^{3-} cotransporter 1	Expression in heart	>0.005	No change	Decreased	No change
87788_at	*RHOQ*	Ras homolog gene family, member Q	Expression in DCM, correlation with BNP ($r = 0.711$)	>0.005	No change	No change	No change
78801_at	*STK38*	Serine/threonine kinase 38	Kinase activity, correlation with PAP ($r = 0.736$)	>0.005	No change	No change	No change

PAP, pulmonary artery pressure; GPCR, G-protein-coupled receptor; CHF, congestive heart failure; BNP, brain natriuretic peptide; CVD, cardiovascular disease; MI, myocardial infarction; DCM, dilated cardiomyopathy; PA, phenylalanine. *p* value indicates the significance of the difference between the gene expression level of failing and non-failing myocardium.

gene promoted [^{3}H]phenylalanine incorporation; and the overexpression of six genes lowered the viability of cardiomyocytes, which was evaluated by Alamar blue assay. We also evaluated the phenotype of transfected cardiomyocytes. Unlike control cells, *MYLK3*-adenovirus-transfected cardiomyocytes were spike shaped. The overexpression of *GPR37L1* induced apoptosis of cardiomyocytes. The transfection of *NBC1*-adenoviral vectors modified the beating rate of cardiomyocytes (data not shown). Then, we analyzed each gene that encoded a distinct cardiomyocyte phenotype by developing gene-targeted mouse models.

In vivo analysis using transgenic and knockout mice

To study the *in vivo* role of the selected genes, we developed genetically modified mice: three transgenic (Tg) mice for *Mylk3*, *Gpr37l1*, or *Nbc1* and three knockout (KO) mice for *Gpr37l1*, *Gpr35*, or *Mmp23*. We estimated hemodynamic parameters using Miller catheter and the heart weight (HW)/body weight (BW). As shown in Fig. 2A, we found that the blood pressure of *Gpr37l1*-KO mice was significantly higher than that of *Gpr37l1*-Tg mice by 61.7 mmHg ($p < 0.01$). Further, the blood pressure of *Gpr35*-KO mice was higher than that of wild type (WT) littermate by 37.5 mmHg ($p < 0.01$). Overexpression with or knockout of *Mylk3*, *Mmp23*, or *Nbc1* did not result in a significant change in the systolic blood pressure. The HW/BW of *Mylk3*-Tg mice was lower than that of *Mylk3*-WT mice (Fig. 2B). The HW/BW was higher in *Gpr37l1*-KO mice than in *Gpr37l1*-Tg mice. The HW/BW in mice with *Nbc1*, *Gpr35*, or *Mmp23* manipulations did not show any difference. These data showed that modification of *Gpr37l1*, *Gpr35*, or *Mylk3* can produce a distinct cardiovascular phenotype *in vivo*.

Discussion

The present study identified heart failure-related genes using a novel strategy that was different from the conventional microarray analysis approach. Firstly, we constructed global gene expression profiles to analyze the gene expression in 12 human samples of failing myocardium and two samples of non-failing myocardium. Secondly, we prepared datasets of heart failure-related genes associated with the severity of heart failure; this approach is unique to our study and has not been published before. Thirdly, we selected four genes from these datasets by microarray analysis and a literature-based search. We also included four orphan GPCR genes and four other genes with high expression in the heart as possible drug targets for heart failure treatment. Fourthly, we screened the *in vitro* functions of these 12 genes by achieving adenovirus-mediated overexpression of these genes in rat cardiomyocytes. Finally, we generated gene-targeted mouse models of the five selected genes and screened the *in vivo* functions of these genes. Our novel strategy using a microarray analysis revealed three potential targets, namely, *MYLK3*, *GPR37L1*, and *GPR35* for diagnosing and managing heart failure.

End-stage heart failure caused by a variety of cardiovascular diseases including hypertension, cardiomyopathy, and ischemic heart disease features a common phenotype of reduced cardiac function and dilated cardiac chamber. This result strongly suggested the existence of common genes during the development of heart failure, including the genes encoding natriuretic peptides. To identify novel diagnostic or therapeutic targets for heart failure, such as natriuretic peptides, several microarray analyses of genes expressed in failing myocardium have been performed in the last decade by comparing the gene expression levels between different pairs of samples, such as non-failing versus failing hearts [4–6], failing hearts before versus after placement of left-ventricular assisting device [7,8], hypertrophic versus failing hearts [9], ischemic versus non-ischemic hearts [10]. However, the severity of heart failure is not fixed, but varies from mild to severe heart failure in these studies. To identify the therapeutic targets for heart failure effectively, we believe that it is important to consider the severity of heart failure with microarray data analysis. In this study, we prepared new datasets of heart failure-associated genes that were selected from gene expression profiles of 12 human failing myocardial samples using clinical parameters. A number of genes were associated with PAP, which is an index for the severity of heart failure, whereas only two genes correlated with EF, which is an index for cardiac contractility. This result implies that the stress caused to the heart, and not the ability of cardiac contraction, regulates gene expression in heart failure. We also selected heart failure-related genes whose expression correlated to

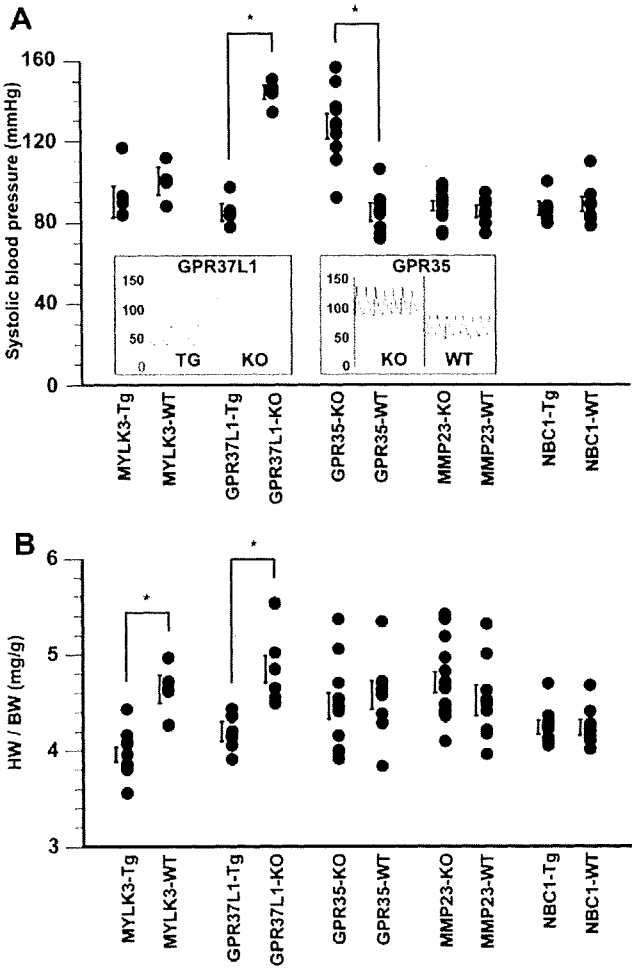

Fig. 2. *In vivo* functional analysis using gene-targeting mice of the *Mylk3*, *Gpr37l1*, *Gpr35*, *Mmp23*, and *Nbc1* genes. Blood pressure and heart weight (HW)/body weight (BW) of transgenic (Tg), knockout (KO) and their wild type (WT) littermate mice of each gene were investigated. Values are means ± SEM. $^{*}p < 0.01$. (A) Systolic blood pressure measured using Millar catheter inserted via right carotid artery. The monitoring chart shows representative data of *Gpr37l1*- and *Gpr35*-manipulated mice. (B) HW/BW ratio of each gene-targeting mouse.

the BNP mRNA level, which is the best known indicator of heart failure. The approach used in our study can help in efficient identification of the diagnostic or therapeutic targets for heart failure rather than only comparing two types of samples such as failing versus non-failing myocardium. Among the genes from these new datasets, we focused on the genes exhibiting high expression in heart tissues and finally selected four genes for performing the screening of functional analysis *in vitro*. The expression level of *MYLK3* gene was highly correlated to PAP, and this gene was detected only in the heart tissue. Recently, we reported that *MYLK3* plays a crucial role in sarcomere assembly via phosphorylation of myosin regulatory light chain 2V (MLC2v) [13]. We also showed that the knockdown of *MYLK3* by using a morpholino oligo caused immature sarcomere formation leading to ventricular dilation in zebrafish. These results indicate that *MYLK3* is strongly associated with the pathophysiology of heart failure. Chan et al. also reported that MYLK3 phosphorylates MLC2v and regulates sarcomere organization [15]. These reports affirm the reliability of our original strategy that involves the microarray analysis of failing myocardium. Among these genes, most genes including *XPR1*, *PRDX4*, and *SMOC2* have not been reported to link with cardiovascular phenotypes and were not included in many gene expression profiles published previously.

Next, we performed *in vivo* functional analysis of five selected genes, and we found that gene-targeted mouse models of *Mylk3*, *Gpr37l1*, or *Gpr35* showed the cardiovascular phenotype. As described above, *Mylk3* plays a crucial role in failing heart. In this study, we identified two GPCRs, namely, *Gpr37l1* and *Gpr35*, whose modification affects systolic blood pressure or HW/BW. To our knowledge, this is the first report about the role of these genes in cardiovascular system.

GPCRs constitute one of the largest protein families, but many GPCRs remain to be orphaned. GPR35 is now known to have some ligands such as kynurenic acid (KYNA) [16], zaprinast [17], and 5-nitro-2-(3-phenylpropylamino) benzoic acid [18]. These agonists mobilize intracellular calcium concentration. Therefore, lowering systolic blood pressure in *Gpr35*-KO mice can be induced by modulating calcium release from calcium-storing organelles. Among the three agonists, only KYNA is produced endogenously as a metabolite of tryptophan. Although GPR35 gene expression is supposed to be specific to immune cells and gastrointestinal tract, we found that GPR35 gene expression increased in failing myocardium. In an inflammatory state, interferon γ induces idolemine 2,3-dioxygenase, a rate-limiting enzyme involved in tryptophan degradation, resulting in a substantial increase in KYNA. Inflammation is thought to be involved in the pathogenesis of dilated cardiomyopathy as well as myocardial infarction. Hence there is a possibility that a KYNA-GPR35 signaling plays a role in the pathogenesis of cardiovascular diseases.

Unlike GPR35, GPR37L1 is still orphaned. However, we found that *Gpr37l1*-KO mice showed significant high blood pressure and high HW/BW as compared to Tg mice, which implies the existence of cardiovascular-related function of *Gpr37l1*. Identification of the ligand and the function of this orphan receptor are awaited.

Although no significant phenotype was observed in *Mmp23* and *Nbc1*-Tg mice, we have been investigating their cardiac function in pathological condition such as myocardial infarction or hypertension and determined their detrimental effect on heart failure (data not shown).

In the present study, we determined 12 novel heart failure-related genes by integrating an original method with parameters that indicated disease severity. Further, we assessed these possible targets of drug discovery. *MYLK3*, *GPR37L1*, and *GPR35* were the newly identified targets that play an interesting role in the cardiovascular system.

Acknowledgments

This study was supported by Grant-in-Aid for Scientific Research (C) in Japan Society for the Promotion of Science; a grant from Human Genome Tissue Engineering and Food Biotechnology in Health and Labor Science Research from the Ministry of Health, Labor, and Welfare, Japan; and a grant from Japan Cardiovascular Research Foundation.

Appendix A. Supplementary data

Supplementary data associated with this article can be found, in the online version, at doi:10.1016/j.bbrc.2010.01.076.

References

[1] Effect of enalapril on survival in patients with reduced left ventricular ejection fractions and congestive heart failure. The SOLVD Investigators, N. Engl. J. Med. 325 (1991) 293–302.
[2] Effect of metoprolol CR/XL in chronic heart failure: metoprolol CR/XL randomised intervention trial in congestive heart failure (MERIT-HF), Lancet 353 (1999) 2001–2007.

[3] M. Packer, M.R. Bristow, J.N. Cohn, W.S. Colucci, M.B. Fowler, E.M. Gilbert, N.H. Shusterman, The effect of carvedilol on morbidity and mortality in patients with chronic heart failure. U.S. Carvedilol Heart Failure Study Group, N. Engl. J. Med. 334 (1996) 1349–1355.
[4] J. Yang, C.S. Moravec, M.A. Sussman, N.R. DiPaola, D. Fu, L. Hawthorn, C.A. Mitchell, J.B. Young, G.S. Francis, P.M. McCarthy, M. Bond, Decreased SLIM1 expression and increased gelsolin expression in failing human hearts measured by high-density oligonucleotide arrays, Circulation 102 (2000) 3046–3052.
[5] J.D. Barrans, P.D. Allen, D. Stamatiou, V.J. Dzau, C.C. Liew, Global gene expression profiling of end-stage dilated cardiomyopathy using a human cardiovascular-based cDNA microarray, Am. J. Pathol. 160 (2002) 2035–2043.
[6] F.L. Tan, C.S. Moravec, J. Li, C. Apperson-Hansen, P.M. McCarthy, J.B. Young, M. Bond, The gene expression fingerprint of human heart failure, Proc. Natl. Acad. Sci. USA 99 (2002) 11387–11392.
[7] B.C. Blaxall, B.M. Tschannen-Moran, C.A. Milano, W.J. Koch, Differential gene expression and genomic patient stratification following left ventricular assist device support, J. Am. Coll. Cardiol. 41 (2003) 1096–1106.
[8] J.L. Hall, E.J. Birks, S. Grindle, M.E. Cullen, P.J. Barton, J.E. Rider, S. Lee, S. Harwalker, A. Mariash, N. Adhikari, N.J. Charles, L.E. Felkin, S. Polster, R.S. George, L.W. Miller, M.H. Yacoub, Molecular signature of recovery following combination left ventricular assist device (LVAD) support and pharmacologic therapy, Eur. Heart J. 28 (2007) 613–627.
[9] J. Rysa, H. Leskinen, M. Ilves, H. Ruskoaho, Distinct upregulation of extracellular matrix genes in transition from hypertrophy to hypertensive heart failure, Hypertension 45 (2005) 927–933.
[10] M.M. Kittleson, S.Q. Ye, R.A. Irizarry, K.M. Minhas, G. Edness, J.V. Conte, G. Parmigiani, L.W. Miller, Y. Chen, J.L. Hall, J.G. Garcia, J.M. Hare, Identification of a gene expression profile that differentiates between ischemic and nonischemic cardiomyopathy, Circulation 110 (2004) 3444–3451.
[11] A.S. Barth, R. Kuner, A. Buness, M. Ruschhaupt, S. Merk, L. Zwermann, S. Kaab, E. Kreuzer, G. Steinbeck, U. Mansmann, A. Poustka, M. Nabauer, H. Sultmann, Identification of a common gene expression signature in dilated cardiomyopathy across independent microarray studies, J. Am. Coll. Cardiol. 48 (2006) 1610–1617.
[12] M. Asakura, M. Kitakaze, Global gene expression profiling in the failing myocardium, Circ. J. 73 (2009) 1568–1576.
[13] O. Seguchi, S. Takashima, S. Yamazaki, M. Asakura, Y. Asano, Y. Shintani, M. Wakeno, T. Minamino, H. Kondo, H. Furukawa, K. Nakamaru, A. Naito, T. Takahashi, T. Ohtsuka, K. Kawakami, T. Isomura, S. Kitamura, H. Tomoike, N. Mochizuki, M. Kitakaze, A cardiac myosin light chain kinase regulates sarcomere assembly in the vertebrate heart, J. Clin. Invest. 117 (2007) 2812–2824.
[14] M. Asakura, M. Kitakaze, S. Takashima, Y. Liao, F. Ishikura, T. Yoshinaka, H. Ohmoto, K. Node, K. Yoshino, H. Ishiguro, H. Asanuma, S. Sanada, Y. Matsumura, H. Takeda, S. Beppu, M. Tada, M. Hori, S. Higashiyama, Cardiac hypertrophy is inhibited by antagonism of ADAM12 processing of HB-EGF: metalloproteinase inhibitors as a new therapy, Nat. Med. 8 (2002) 35–40.
[15] J.Y. Chan, M. Takeda, L.E. Briggs, M.L. Graham, J.T. Lu, N. Horikoshi, E.O. Weinberg, H. Aoki, N. Sato, K.R. Chien, H. Kasahara, Identification of cardiac-specific myosin light chain kinase, Circ. Res. 102 (2008) 571–580.
[16] J. Wang, N. Simonavicius, X. Wu, G. Swaminath, J. Reagan, H. Tian, L. Ling, Kynurenic acid as a ligand for orphan G protein-coupled receptor GPR35, J. Biol. Chem. 281 (2006) 22021–22028.
[17] Y. Taniguchi, H. Tonai-Kachi, K. Shinjo, Zaprinast, a well-known cyclic guanosine monophosphate-specific phosphodiesterase inhibitor, is an agonist for GPR35, FEBS Lett. 580 (2006) 5003–5008.
[18] Y. Taniguchi, H. Tonai-Kachi, K. Shinjo, 5-Nitro-2-(3-phenylpropylamino)-benzoic acid is a GPR35 agonist, Pharmacology 82 (2008) 245–249.